Chinese Chemical Letters 35 (2024) 108900

Contents lists available at ScienceDirect

Chinese Chemical Letters

journal homepage: www.elsevier.com/locate/cclet

Recent advances in iron-based sulfides electrocatalysts for oxygen and hydrogen evolution reaction

Jing Mei[a,b], Yuqing Deng[a,b], Xiaohong Cheng[c,*], Xing Wang[a,*], Qi Wu[a,b,*]

[a] State Key Laboratory of New Textile Materials and Advanced Processing Technologies, Wuhan Textile University, Wuhan 430200, China
[b] Hubei Key Laboratory of Pollutant Analysis & Reuse Technology, College of Chemistry and Chemical Engineering, Hubei Normal University, Huangshi 435002, China
[c] Hubei Key Laboratory of Low Dimensional Optoelectronic Materials and Devices, Hubei University of Arts and Science, Xiangyang 441053, China

ARTICLE INFO

Article history:
Received 13 April 2023
Revised 28 May 2023
Accepted 7 August 2023
Available online 9 August 2023

Keywords:
Iron-based sulfides
Electrocatalysts
Doping
Composites
Water splitting

ABSTRACT

Increasing environmental pollution and shortage of conventional fossil fuels have made it urgent to develop renewable and clean energy sources. Electrocatalytic water splitting, with its abundant raw materials, simple process, and zero carbon emission, is considered one of the most promising processes for producing carbon-neutral hydrogen which has excellent energy conversion efficiency and high gravimetric energy density. Among them, oxygen evolution reaction (OER) electrocatalysts and hydrogen evolution reaction (HER) electrocatalysts are critical to decreasing the intrinsic reaction energy barrier and boosting the hydrogen evolution efficiency. Therefore, it is imperative to develop and design low-cost, highly active, and stable OER and HER electrocatalysts to lower the overpotential and drive the electrocatalytic reactions. Transition metal sulfides, especially iron-based sulfides, have attracted extensive exploration by researchers as a result of its high abundance in the Earth's crust and near-metallic conductivity. Consequently, in this review, we systematically and comprehensively summarize the progress in the application of iron-based sulfides and their composites as OER and HER electrocatalysts in electrocatalysis. Detailed descriptions and illustrations of the special relationships among their composition, structure, and electrocatalytic performance are presented. Finally, this review points out the challenges and future prospects of iron-based sulfides in practical applications for designing and fabricating more promising iron-based sulfide OER and HER electrocatalysts. We believe that iron-based sulfide materials will have a wide range of application prospects as OER and HER electrocatalysts in the future.

1. Introduction

At present, environmental pollution and energy exhaustion as the top ten global crises that have attracted widespread attention. At the same time, the accelerated consumption of traditional fossil energy sources such as coal, oil, and natural gas has caused irrevocable damage to the ecological environment while promoting the rapid development of our economy [1–7]. For this reason, it is an urgent need to explore and develop more renewable and environmentally friendly clean energy sources. It has become one of the ideal solutions to cope with the energy and environmental crisis, as well as to build a clean, low-carbon, and efficient modern energy system in the world [8–13]. In recent years, renewable energy sources such as wind, solar, tidal, and bioenergy have been extensively applied in our daily life. Nevertheless, the generation of these energy sources is not only affected by natural conditions such as day and night, season, geographical latitude, and sea-level height but also limited by economic conditions such as inefficiency and high cost, which makes it difficult to meet the demand of power supply for large-scale production throughout the day [14–20]. In contrast to these intermittent, local, and climatic energy sources, hydrogen energy, with its excellent energy conversion efficiency and higher gravimetric energy density than gasoline, has been widely recognized as the most promising clean energy source to replace non-renewable fossil fuels [21–25]. Both steam reforming or partial oxidation of hydrocarbons and coal gasification are still widely developed and applied means of hydrogen production. Nevertheless, this hydrogen production process not only consumes a large number of fossil fuels and increases the energy pressure, but also produces harmful gases such as carbon dioxide, which causes irreversible secondary pollution to the environment [26–33]. Therefore, in recent years, the generation of

* Corresponding authors.
E-mail addresses: chengxiaohong0807@126.com (X. Cheng), wx@wtu.edu.cn (X. Wang), wuqi2011@whu.edu.cn (Q. Wu).

https://doi.org/10.1016/j.cclet.2023.108900
1001-8417/

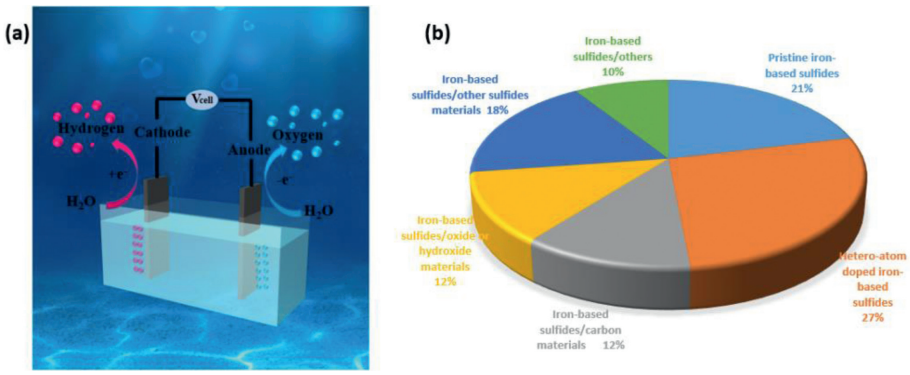

Fig. 1. (a) Schematic diagram of electrocatalytic oxygen and hydrogen evolution reaction (OER and HER). (b) Pie chart of the percentage of different iron-based sulfides materials as electrocatalysts for OER and HER.

hydrogen by electrochemical water splitting has emerged as the ideal way to achieve efficient energy utilization and storage, due to its advantages of using the earth's abundant water as feedstock, zero CO_2 emission, low cost, and efficient hydrogen production, and high purity of hydrogen production among various large-scale hydrogen generation technologies [34–39]. Unfortunately, it is still greatly hindered in practical production applications.

The electrochemical water splitting consists of two main half-reactions, namely the water reduction hydrogen evolution reaction (HER) at the cathode and the water oxidation oxygen evolution reaction (OER) at the anode [35,40-44]. Theoretically, a theoretical thermodynamic potential energy of 1.23 V is required to drive the overall water splitting to produce hydrogen and oxygen [45,46]. Yet, the actual process in which the OER and HER reactions occur requires overcoming the inherent activation obstacles of the anode (η_a) and cathode (η_c), as well as other unavoidable hindrance (η_{other}) caused by the electrolyte-electrode contact, which makes the actually operational potential much higher than the theoretical one [3,47-51]. Consequently, it is urgently necessary to design and develop efficient and stable electrocatalysts to reduce this energy barrier and accelerate the reaction kinetics so that the overall water splitting for hydrogen production technology can be perfected.

To date, noble metal Ru/Ir-based materials and Pt-based materials are considered to be the most efficient OER and HER electrocatalysts, respectively [52–55]. Unfortunately, noble metal-based materials are greatly limited by the scarcity of sources and high costs in practical production applications [56–60]. As a result, it is necessary to find a cheap and efficient electrocatalyst to facilitate the further development of OER and HER technologies. In recent years, with the continuous improvement and development of production technology levels, as alternatives to precious metal-based materials, non-precious metal-based electrocatalysts with abundant earth content, such as transition metals (Fe, Co, Ni, Cu, W) and their alloys [41,61-63], oxides [64–66], hydroxides [67–70], phosphides [71–74], sulfides [75–77], and nitrides [78–80] have been received wide attention regarding their outstanding OER and HER catalytic activity, low cost, and easy availability.

Among the above non-precious metal-based materials, transition metal sulfides (TMSs) have enjoyed world-wide research attention due to their unique electronic orbital structure, two-dimensional structures, low cost, modifiable electronic properties and compositions, and abundant active sites [81–84]. Moreover, compared with other TMSs, iron-based materials are regarded as promising alternatives to noble metal-based materials for their advantages such as simple preparation, high natural abundance, low cost, and similar catalytic mechanism with [Fe-Fe] hydrogenase [85–88]. Therefore, recently, the research on iron-based sulfide compounds as OER and HER electrochemical catalysts has made great progress, and it is necessary to summarize the development of their study.

Meanwhile, S (sulfur) atoms are considered to play a crucial role in the excellent electrocatalytic performance of TMS since they can promote the formation of unique structures and abundant active species in the catalyst during electrochemical processes [76,89-91]. Compared with other TMSs, iron-based sulfides electrocatalysts have a bright application prospect: (1) Transition metal Fe element as the most abundant metal element in the earth's crust, have significant advantages such as high natural abundance and low cost [92]; (2) Iron-based sulfides, a natural metal sulfide, exhibits excellent electrocatalytic performance in HER owing to the similar electrocatalytic mechanism with high active native [Fe-Fe] hydrogenase [93,94]; (3) The synthesis method of iron-based sulfides is simple and time-saving, which is also one of the outstanding advantages of Fe-based sulfide materials [95]; (4) Iron-based sulfides electrocatalysts contain a large amount of Fe-Fe and Fe-S bonds, which are beneficial to promote the formation of *OOH intermediates during OER process and the combination of *H intermediates to form H_2 during HER process [76,96-98]; (5) The continuous network of Fe-Fe bonds makes them exhibit metallic properties with better electrical conductivity, which facilitates rapid charge transfer [99,100]. Because of these properties, iron-based sulfides are considered to be excellent candidates for non-noble metal-based electrocatalysts. Nevertheless, to date, there have been few targeted reviews on iron-based sulfide electrocatalysts and optimization strategies to improve their electrocatalytic performance. Therefore, an in-depth summary of the research progress on non-precious metal iron-based sulfide electrocatalysts for OER and HER applications is necessary.

This paper reviews the research advancement of iron-based sulfide electrochemical catalysts, mainly including FeS, FeS_2, Fe_7S_8 and their composites, as well as their application in electrochemical hydrogen evolution reactions and oxygen evolution reactions in recent years. The composition, structure, and electrochemical catalytic performance of the catalysts are systematically summarized, as shown in Fig. 1. In addition, potential challenges in the development of iron-based sulfide electrocatalysts are discussed, and some suitable and effective suggestions are made for their future development prospects. It is hoped that the review in this paper will provide practical solutions for the subsequent design and development of new high-performance and low-cost iron-based sulfide electrocatalysts for actual applications in this field.

2. The synthesis of iron-based sulfides electrocatalysts

The morphology, material size, and composition of iron-based sulfide electrocatalysts are affected to diverse degrees by differ-

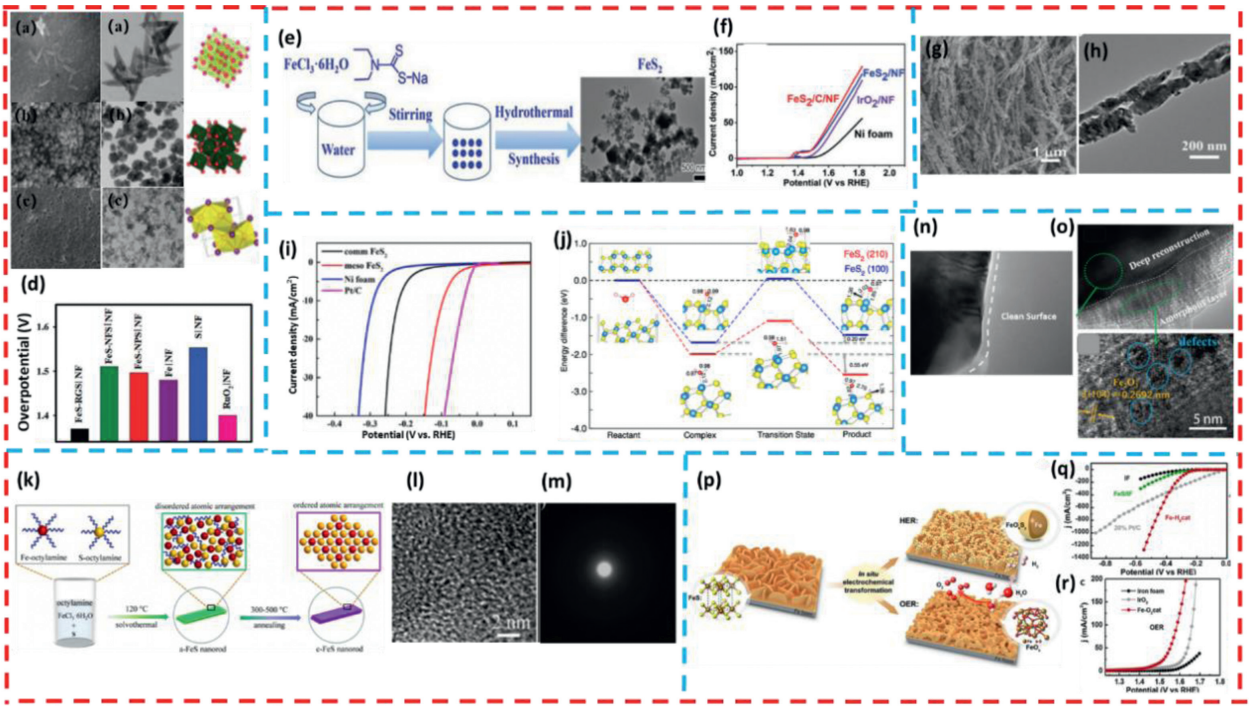

Fig. 2. SEM and TEM images of (a) FeS-RGS, (b) FeS-NFS and (c) FeS-NPS. (d) Comparison of the overpotential of different samples. Copied with permission [94]. Copyright 2021, The Royal Society of Chemistry. (e) The synthetic pathway for the FeS_2 NPs. (f) LSV curves of overall water splitting in 1.0 mol/L KOH by using FeS_2/C/NF as both the cathode and anode. Copied with permission [105]. Copyright 2018, The Royal Society of Chemistry. (g) SEM and (h) TEM image of FeS_2/C nanowires. Copied with permission [103]. Copyright 2021, Elsevier. (i) HER polarization curves of the mesoporous FeS_2. (j) Reaction pathways for O-H bond breaking of H_2O molecule on (210) (red line) and (100) (blue line) surfaces. Copied with permission [110]. Copyright 2020, Wiley-VCH GmbH. (k) Schematic illustration of the synthesis of a-FeS and c-FeS nanorods. (l) HRTEM and (m) SAED pattern of a-FeS nanorods. Copied with permission [102]. Copyright 2019, Multidisciplinary Digital Publishing Institute. HRTEM image of (n) FeS_2 pre-catalyst and (o) the amorphous/crystalline hybrid FeS_2 catalyst. Copied with permission [111]. Copyright 2020, World Scientific. (p) Schematic illustration of FeS/IF as a pre-catalyst for generating active electrocatalysts for both HER and OER. (q, r) LSV curves for HER and OER in 1 mol/L KOH solution (without iR correction). Copied with permission [87]. Copyright 2018, Elsevier.

ent synthesis methods, thus significantly improving their OER and HER catalytic performance. In recent years, with the development of diverse technologies and a better understanding of iron-based sulfide electrocatalysts, a wide variety of methods have been used for the synthesis of different iron-based sulfide nanomaterials. The main types of sulfidation methods are as follows: (1) Hydrothermal: For iron-based sulfides, owing to their controlled composition and structure, they are usually synthesized by hydrothermal methods using solutions containing sulfur sources and metal salt precursors containing Fe or iron metal substrate materials (iron foam). The composition and structure can be modified by adjusting the ratio of Fe and the reaction temperature/pressure. For instance, Zou *et al.* [87] synthesized FeS/IF nanosheet arrays using thiourea as the sulfur source to directly sulfide on IF. After HER electrochemical activation, a large number of nanoparticles were generated *in situ* on FeS/IF nanosheets; porous amorphous FeO_x films were formed after OER activation. (2) Electrodeposition method: This method involves the transfer of positive and negative ions in an electrolyte solution under the action of an external electric field, as well as the formation of a plating layer by the redox reaction of electrons at the electrode. When metal cations are generated on the cathode to form a metal coating, it is called electroplating; when metal oxidation occurs on the anode to form an oxide film, it is called electrochemical oxidation. For example, Elakkiya *et al.* [94] immersed the pretreated NF in an electrolytic mixture of 5.0 mmol/L $Fe(NO_3)_3{\cdot}9H_2O + 7.0$ mL DMSO + 0.1 mol/L HNO_3 and scanned it for 5 cycles between −0.163 V and 1.63 V using the CV method. The SEM image of Fig. 2a shows that the FeS-RGS/NF obtained by electrodeposition has a rice-like morphology, which has high surface area and abundant defective active sites. For instance, Tan *et al.* [101] prepared FeS/FeO_xH@Fe nanosheets directly by one-step electrodeposition, using $FeSO_4{\cdot}7H_2O$ and thiourea as the iron and sulfur sources, respectively, and electrodeposited 240 s at a current density of 300 mA/cm^2. The crystalline and amorphous interfacial structures were formed by a simple one-step co-deposition method, which resulted in excellent electrical conductivity and stability. (3) Solvothermal method: For example, Zhang *et al.* [102] used an octylamine solvent to promote the formation of amorphous structures, resulting in prepared a-FeS nanorods with more defective active sites and larger active specific surface area. The octylamine solvent acts as a reducing agent for Fe^{3+} and S on the one hand, and as a capping agent covering the catalyst surface on the other hand, which prevents the directional growth of nuclei and facilitates the generation of amorphous structures with highly disordered atomic arrangements. $FeCl_3{\cdot}H_2O$ and S react with the octylamine solvent to form the corresponding complexes, respectively, and then react with each other to form a-FeS at high temperature. For instance, Pan *et al.* [103] used ethylenediamine and ethylene glycol as solvents to prepare FeS_2-coordinates precursors in which the decomposition of organic molecules in subsequent reactions led to the creation of a large number of voids in the carbon shells of nanowires, which facilitated the generation of more active sites and the rapid transfer of electrons. (4) Chemical vapor deposition (CVD): This method refers to the deposition of hydrogen sulfide gas or sublimated sulfur onto a solid precursor substrate of heated metal compounds or metal elements after several reactions at high temperatures, and this method is suitable for preparing thin sheets or nanoblocks with high crystallinity on the substrate. For example, Chen *et al.* [104] first prepared α-Fe_2O_3@C precursors by a two-part hydrothermal reaction, and subsequently

prepared γ-Fe_2O_3@FeS_2@C by partially sulfidation the precursors with S powder in a 1:3 ratio by annealing in a tube furnace at 600 °C.

3. Pristine iron-based sulfides electrocatalysts for OER and HER

In recent years, iron-based sulfides (FeS, FeS_2, Fe_7S_8, *etc.*) have been demonstrated to be excellent OER and HER electrocatalysts. It is well known that nanostructured electrocatalysts with high specific surface area are widely used in OER and HER due to the fact that constructing a favorable morphology can obtain a larger specific surface area than the native material and expose more effective active sites for higher catalytic efficiency. Currently, various nanostructured iron sulfide materials have been synthesized and applied in the field of electrocatalysis, such as zero-dimensional (0D) nanoparticles (NPs), one-dimensional (1D) nanowires (NWs), two-dimensional (2D) nanofilms/sheets (NSs) and three-dimensional (3D) network structures.

For example, by using $Fe(NO_3)_3{\cdot}9H_2O$ and dimethyl sulfoxide (DMSO) as the iron and sulfur sources, respectively, Rajasekaran Elakkiya and his colleagues [94] prepared a series of different morphologies (rice seeds, flowers and NPs) of FeS with three different synthetic strategies, namely electrodeposition, solvothermal and chemical reduction, to modulate the morphology of ferrous sulfide FeS (Figs. 2a-c). The rice-like FeS (FeS-RGS) nanomaterial prepared by electrodeposition is found to exhibit good OER catalytic activity in alkaline media. When FeS-RGS is used as the anode material, only an overpotential of 0.20 V is required to achieve a current density of 10 mA/cm^2 with a Tafel slope of 54.2 mV/dec (Fig. 2d). The excellent OER electrocatalytic performance can be attributed to its unique rice-like morphology, which exhibit high active specific surface area and abundant active defect sites.

Li *et al.* [105] prepared FeS_2/C NPs by a simple hydrothermal method using $C_5H_{10}NS_2Na{\cdot}3H_2O$ as the sulfur source and $FeCl_3{\cdot}6H_2O$ as the iron source (Figs. 2e and f). Electrochemical performance tests reveal that FeS_2/C/NF NPs grown on conductive substrate Ni foam have excellent OER and HER electrocatalytic activities. The morphology of the nanoparticles allows for a larger specific surface area and thus more active sites, which can promote the charge and mass transfer rates of the OER and HER reaction processes, thereby improving activity and stability.

In addition to the morphology, porosity is also an essential factor that affects the electrocatalytic performance of the materials. Consequently, porous and mesopore materials facilitate rapid charge/mass transfer due to their exposure of large active surface areas, thus improving the electrocatalytic activity of the materials [106–109]. For example, Pan *et al.* [103] synthesized FeS_2-ethylenediamine nanowire precursors by hydrothermal method and then pyrolyzed them to obtain FeS_2/C catalysts with porous nanostructures. The pyrolysis of organic groups produced many pores in the carbon shell of the nanowires, which provided abundant active sites for the OER reaction and channels for rapid electron transfer (Figs. 2g and h). More importantly, after electrochemical activation, FeS_2/C exhibited good OER catalytic activity with overpotentials of 291 mV and 338 mV required to reach current densities of 10 mA/cm^2 and 50 mA/cm^2, respectively, and could be stabilized for 15 h.

Miao *et al.* [110] prepared an efficient mesoporous iron disulfide nanoparticle material that could operate stably under alkaline conditions by using a facile inverse micellar sol-gel method and low-temperature sulphuration method. Benefiting from the mesoporous structure, the obtained mesoporous FeS_2 has a high specific surface area and abundant active sites, which are favorable for charge transfer and mass transport. The polarization curves shows that the mesoporous FeS_2 with low overpotential has better HER performance (96 mV@10 mA/cm^2) under 1.0 mol/L KOH conditions. Furthermore, the analysis of the results based on the density function theory (DFT) calculations (Figs. 2i and j) shows that the activation barrier EA of the (210) crystal plane (0.89 V) is lower than that of the (110) (1.46 V), which is more easily subjected to water splitting reaction. And the transition state energy value of (210) surface is calculated to −1.09 V, which is lower than that of (110) surface (−0.21 V). In summary, mesoporous FeS_2 possesses superior catalytic activity for hydrogen production.

The inherent electrocatalytic activity of iron-based sulfides can be effectively modified by phase modulation. Pure amorphous phases are inherently contained rich defects, making them favorable in the adsorption of OH* and the formation of OOH*. For example, Zhang *et al.* [102] synthesized an amorphous $Fe_{0.95}S_{1.05}$(a-FeS) nanorods using a facile solvothermal method (Fig. 2k). The highly disordered arrangement of the atoms and the amorphous nature can be seen in Figs. 2l and m. The obtained sample shows better HER catalytic activity and long-term stability (67 mV@10 mA/cm^2@80 h) compared to crystalline $Fe_{0.95}S_{1.05}$ (c-FeS). The improved catalytic performance of HER is attributed to the large number of unsaturated atoms in a-FeS amorphous nanorods arranged in a disorderly manner, which exposes a large number of catalytically active sites with surface defects, thus facilitating charge transfer between the electrode and the electrolyte solution.

Amorphous/crystalline hybrid iron disulfide synthesized by surface self-reconstruction is developed for the first time by Wang *et al.* [111] for an OER electrocatalyst. The amorphous/crystalline FeS_2 catalyst is used as the anode to catalyze the oxygen evolution reaction with an overpotential of mV at a current density of 10 mA/cm^2, which is superior to that of commercial RuO_2. The authors pointed out that the outstanding electrocatalytic performances were mainly due to a certain degree of change in the catalyst surface phase, composition and structure before and after the OER reaction, with partial crystalline transformation into an amorphous state with abundant defects (Figs. 2n and o). Notably, through the XPS spectra, it can be found that the ratio of Fe^{3+}/Fe^{2+} increased after the OER reaction. Moreover, the S elements are heavily leached after the OER reaction and abundant sulfates are adsorbed on the catalyst surface. The results indicates that FeS_2 are partially transformed into amorphous $Fe(OH)_x$ or Fe_2O_3 active material, which plays an important role in the high OER catalytic performance.

Zou *et al.* [87] provided some new insights into the electrocatalytic mechanism of FeS in OER and HER (Figs. 2p-r). During electrochemical reduction conversion (HER), the iron near the surface of the FeS nanosheet arrays are reduced to form metal nanoparticles and large leaching of S^{2-}, which are subsequently oxidized, resulting in the *in-situ* generation of a thin sulfur-doped oxide shell layer (Fe@FeO_xS_y) on the Fe nanoparticles. According to various analytical tests, it is confirmed that the presence of S and O atoms in FeO_xS_y increase the electron density of the surface and decrease the Gibbs free energy of intermediate H* adsorption value (ΔG_{H^*}). Therefore, the conversion of the FeS/IF surface into the catalytically active phase Fe@FeO_xS_y can provide more active sites and improve the HER catalytic activity. In the OER process, the sulfur on the FeS surface are consumed and completely replaced by oxygen, resulting in amorphous FeO_xH films with porous structures on IF. The electrocatalytic performance of FeS/IF has been greatly improved using electrochemical activation (243 mV@100 mA/cm^2@HER, 238 mV@10 mA/cm^2@OER).

This section summarizes the application of pristine iron-based sulfide catalysts in OER and HER (Table 1). Based on the above discussion of pristine iron-based sulfide electrocatalysts, we can summarize the following points: Firstly, iron-based sulfide nanoparticles with porous and mesoporous structures have the larger electrocatalytic specific surface area and active sites than pure nanoparticles, making them more favorable for electron/mass

Table 1
Morphology and performance of pristine iron-based sulfides electrocatalysts (The electrolyte is 1.0 mol/L KOH).

Catalyst	Morphology	Working electrode substrate	Overpotential @ current density (mV@mA/cm^2@OER or HER)	Tafel slope (mV/dec)	Stability (h)	Ref.
FeS/IF	Nanosheet arrays	Iron foam	238@10@OER,243@100@HER	77@HER	50	[87]
FeS	Rice-grains-like nanoparticles	RGS	200@10@OER	54.2@OER	15	[94]
$Fe_{0.95}S_{1.05}$ (a-FeS)	Nanorods	/	67@10@HER	43@HER	80	[102]
FeS_2/C	Porous nanowires	/	291@10@OER,338@50@OER	65@OER	15	[103]
FeS_2/C	Nanoparticle	Ni foam	240@10@OER,202@10@HER	98@OER	5	[105]
FeS_2	Mesoporous nanoparticles	/	96@10@HER	78@HER	24	[110]
FeS_2	Hollow-sphere structure	/	189.5@10@OER	71@OER	5	[111]

transfer and thus improving OER and HER performance. Secondly, the disordered arrangement of a large number of unsaturated atoms in amorphous Fe-based sulfides exposes more defective active sites, facilitating charge transfer by more favorable contact between electrolyte solution and electrode. Finally, it is found that iron-based sulfides usually exist as pre-catalysts in electrocatalytic reactions, easily generating iron-based oxides or hydroxides, which are the real active sites of iron-based sulfides in OER and HER reactions.

4. Hetero-atom doped FeS-based electrocatalysts for OER and HER

Heteroatom doping is considered as an effective strategy to modulate the catalytic performance of catalysts from the atomic scale. It can not only optimize the electronic structure and surface composition of iron sulfide nanomaterials with higher electrical conductivity and more effective active sites, but also improve the intrinsic catalytic activity of iron sulfide-based catalysts by optimizing the adsorption energy of catalytic reaction intermediate active species and reducing the free energy of the decisive step of catalytic reaction. Moreover, the synergistic effect between ions will also further improve the electrocatalytic performance. Heteroatom doping is mainly classified into metal doping, anion doping and anion-cation co-doping.

Co atom doping optimizes the electronic and crystal structures of iron sulfide materials, adjusts the position of the d-band center, leads to a significant improvement in electrical conductivity, and therefore accelerates the rate of electron and mass transmission during the catalytic reaction, thus enhancing the electrocatalytic activity of iron sulfide nanomaterials. Gao *et al.* [112] successfully prepared Co-doped FeS_2 nanospheres with porous structures by a simple solvothermal reaction and sulfidation reaction. The catalyst achieves a current density of 10 mA/cm^2 in 1 mol/L KOH requiring only a cell voltage of 1.60 V to drive the overall water splitting (Fig. 3a). Notably, the porous nanosphere structure formed by Co-FeS_2 is beneficial to obtain a larger specific surface area, improve the contact between the material and the electrolyte, and accelerate the rapid diffusion of gas. Wu *et al.* [113] synthesized ultrathin nanosheets of Co-doped Fe_7S_8 ($Co_{13.6\%}$-Fe_7S_8) by a simple hydrothermal and thermal treatment method (Fig. 3b). To achieve a current density of 10 mA/cm^2, it requires only 311 mV and 284 mV for OER and HER. It can be observed by XPS that the electron binding energy of Fe 2p gradually shifts to lower values with increasing Co doping (Fig. 3c), which indicates that the active Co atoms optimize the electronic structure of Fe. Meanwhile, the results of contact angle measurements demonstrate that Co doping improves the adsorption capability of Fe_7S_8 to water in alkaline medium and accelerates the electrolyte delivery and electron transport rate. Consequently, the catalytic efficiency of HER and OER in alkaline medium has been improved by metal Co doping. Wang *et al.* [114] synthesized a sequence of $Fe_{1-x}Co_xS_2$/RGO through a simple thermal injection method. The Fe atoms on the catalytic surface has been partially replaced by Co atoms (Figs. 3d-g). It is indicated that the Fe sites adsorbed hydrogen atoms more easily according to the DFT calculations (Fig. 3h). The ΔG_{H^*} value of the Fe site on the original FeS_2 (001) surface is calculated to 0.65 eV, while after Co doping, the ΔG_{H^*} value of the Fe site decreases to 0.02 eV, which is close to zero. This indicates that the adsorption of hydrogen atoms at Fe sites is significantly enhanced. In summary, Co doping improves the chemical environment of Fe atoms and significantly strengthens the intrinsic catalytic activity of HER. As a result, the low overpotential of HER is 198 mV at 10 mA/cm^2 in 0.5 mol/L sulfuric acid solution.

Jiang and coworkers [115] investigated the effect of doping with different levels of nickel on the HER electrocatalytic performance of FeS_2 nanoparticles on redox graphene ($FeNi_xS_2$-RGO). It was found that the $FeNi_{0.2}S_2$-RGO electrode nanoparticle morphology remained intact when the nickel doping ratio was 20% ($x = 0.2$) and exhibited better HER electrocatalytic performance than the $FeNi_{0.1}S_2$-RGO electrode in 0.5 mol/L H_2SO_4. Yin *et al.* [116] prepared Ni-Fe-S hollow-layered spheres with a layered porous structure through a simple two-step hydrothermal treatment. After the doping of Ni atoms, Ni-Fe-S still maintains a hollow sphere structure similar to the pure Fe-S (Fig. 3i). The red-shifted XPS spectrum of Fe 2p after Ni doping has been observed from XPS (Figs. 3j and k), which indicates that the heteroatom doping changed the surface chemical composition and valence state of Fe atoms. At the same time, the formed porous nanosphere structure discloses more active sites, which together contribute to the enhancement of catalytic performance. Hence, the catalyst exhibits remarkable OER and HER electrocatalytic performances and long-term stability in 1.0 mol/L KOH. Specifically, when the current density is 10 mA/cm^2, it requires only 223 mV and 115 mV of overpotential for OER and HER, respectively. Moreover, the overall water splitting cell which is assembled by Ni-Fe-S exhibits a low cell voltage (1.57 V@10 mA/cm^2) in alkaline medium.

The construction of amorphous structures in two-dimensional layered materials has been shown to be an effective strategy for generating surface reconstruction and increasing the number of active sites. Shao *et al.* [117] successfully prepared ultrathin amorphous two-dimensional Mo-doped FeS nanosheet (Mo-FeS NSs) structures with abundant sulfur vacancy defects by a simple geothermal strategy. It has been found by TEM and SAED mapping that FeS transformed from a layered crystalline structure to an amorphous nanosheet structure after Mo doping, resulting in excellent OER electrocatalytic activity in alkaline media. It exhibits a low overpotential of 210 mV at 10 mA/cm^2 and maintains 30 h stability for OER (Fig. 3l). The effect of Mo doping on the OER activity of Fe-S catalysts has been further understood based on DFT (Figs. 3m and n). The accelerated electron/mass transfer on the oxygen intermediate during the electrochemical reaction can be attributed to the surface remodeling and sulfur-rich vacancy defects caused by the amorphous structure.

In addition, anion doping can also modulate the electronic structure of the catalyst and optimize the adsorption or desorp-

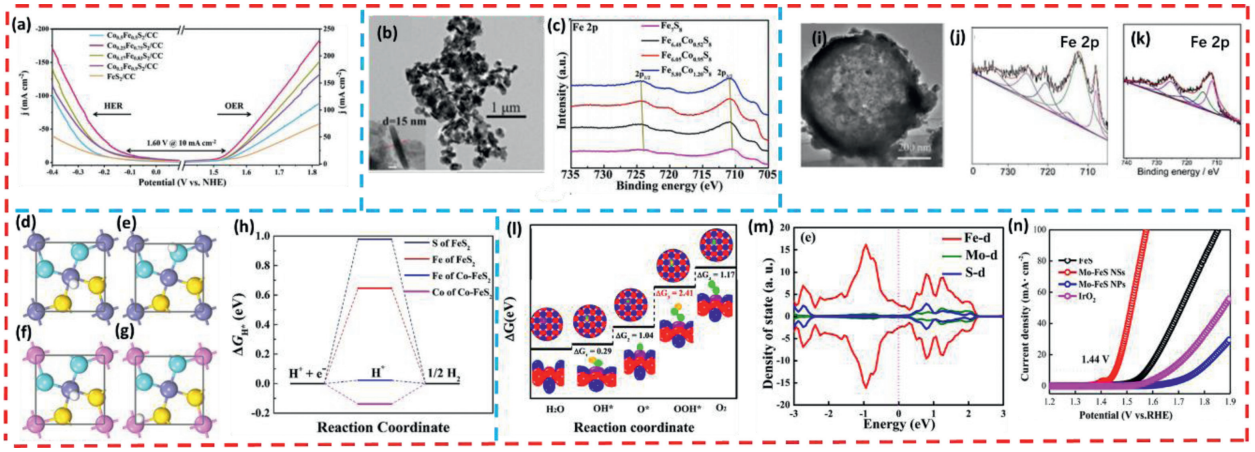

Fig. 3. (a) Polarization curves of Co-FeS_2 for the HER and OER in 1 mol/L KOH solution. Copied with permission [112]. Copyright 2020, The Royal Society of Chemistry. (b) TEM image of $Co_{0.95}Fe_{6.05}S_8$ (Inset exhibits the thickness of nanosheets). (c) XPS survey spectra of Fe_7S_8 and Co-Fe_7S_8. Copied with permission [113]. Copyright 2021, Elsevier. Top views of the adsorbed structures of hydrogen atom near (d) Fe and (e) S sites of pure FeS_2 (001) surface and (f) Fe and (g) Co sites of Co-doped FeS_2 (001) surface. The Fe, Co, S and H atoms are represented as bluish violet, pink, yellow and white spheres, respectively. (h) The calculated ΔG_{H^*} for hydrogen adsorption on Fe and S sites of pure FeS_2 (001) surface and Fe and Co sites of Co-doped FeS_2 (001) surface. Copied with permission [114]. Copyright 2021, Elsevier. (i) low-resolution TEM image of the Ni–Fe–S hierarchical sphere. (j, k) XPS of Fe 2p of Ni-Fe-S before and after OER. Copied with permission [116]. Copyright 2020, American Chemical Society. (l) OER polarization curves of Mo−FeS. (m) Mo−FeS NSs Free energy diagram of three simulated models at $U=0$. (n) Projected DOS of Mo−FeS-NSs. The Fermi level is set to zero. Copied with permission [117]. Copyright 2019, Elsevier.

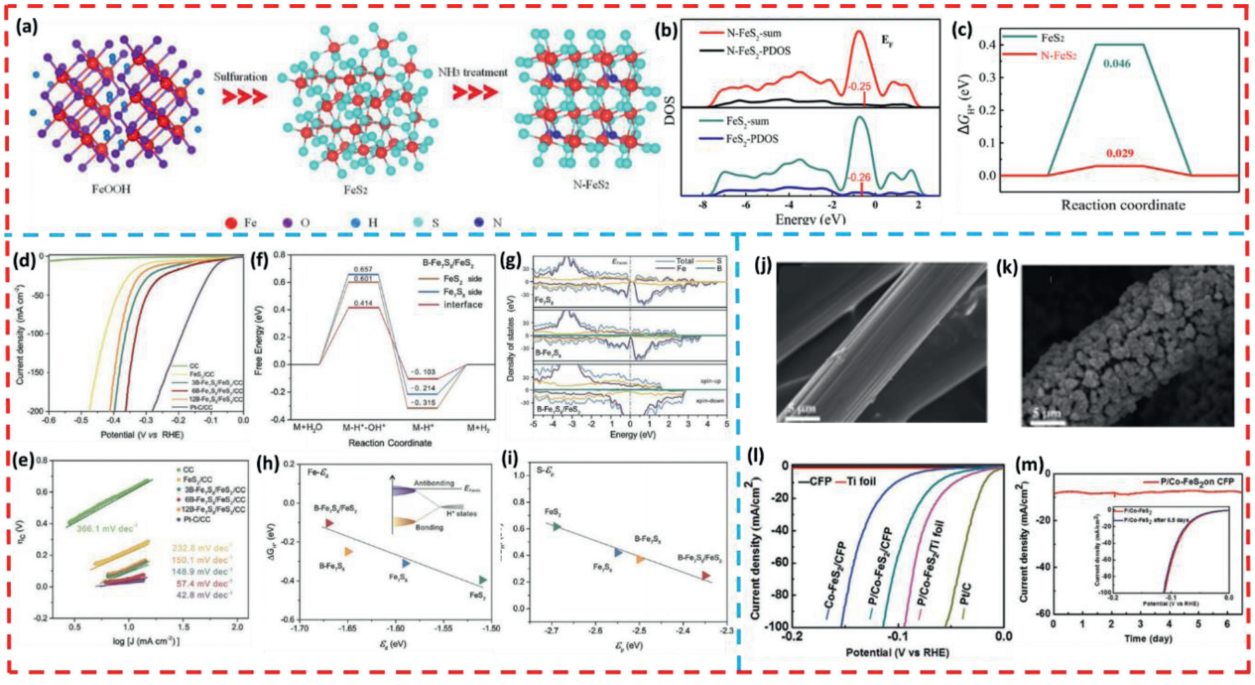

Fig. 4. (a) Simplified schematics of preparation process of N-FeS_2 nanoparticles. DFT calculation of FeS_2 and N-FeS_2: (b) The PDOS plots; (c) Free-energy diagram for the HER. Copied with permission [118]. Copyright 2021, Elsevier. (d) The iR-corrected HER polarization curves and (e) Tafel slopes of the FeS_2/CC, B-Fe_7S_8/FeS_2/CC, and Pt/C-CC electrocatalysts. The DFT calculation results of the B-Fe_7S_8/FeS_2 electrocatalysts: (f) The corresponding free energy diagrams of the B-Fe_7S_8/FeS_2 electrocatalysts toward alkaline HER on the B-Fe_7S_8 side, the FeS_2 side, and the B-Fe_7S_8/FeS_2 heterointerface; (g) The electronic density of states (DOSs). (h) Dependence of free energies of hydrogen adsorption on the d-band centers (εd) of Fe 3d state and (i) the p-band centers (ε_p) of S 3p state. Copied with permission [119]. Copyright 2022, Wiley-VCH GmbH. SEM images of (j) carbon fiber paper (CFP) and (k) P/Co-FeS_2 nanocomposites on CFP. (l) Polarization curves. (m) Current *versus* time during the long term (6.5 d) with constant-potential (−0.07 V) electrolysis of P/Co-FeS_2 catalysts on CFP. Copied with permission [120]. Copyright 2017, Wiley-VCH GmbH.

tion energy of the intermediate, thus improving the intrinsic OER and HER activities of iron sulfide. Owing to the higher electronegativity of N atoms than S atoms, the doping of nitrogen can remarkably boost the performance of the catalyst. Ye *et al.* [118] successfully synthesized nitrogen-doped FeS_2(N-FeS_2) NPs with a simple hydrothermal and CVD method which used sulfur powder and ammonia as the sulfur and nitrogen sources, respectively (Fig. 4a). The optimized N-FeS_2 exhibits favorable HER activity, which requires only a low overpotential of 126 mV to achieve a current density of 10 mA/cm^2 in 1.0 mol/L potassium hydroxide solution with a Tafel slope of 124 mV/dec. To further investigate the effect of N doping on FeS_2, the authors proceed DFT calculations (Figs. 4b and c), the presence of N dopant remarkably increases the total density of states (DOS) around the Fermi energy level, which results in higher electrical conductivity of N-FeS_2. The p-band center of N-FeS_2 (0.25 eV) is slightly higher than that of FeS_2 (0.26 eV) as shown by the surface p-band density of state bias (PDOS) calculation. Consequently, the interaction between H* and the S atoms on

Table 2
Performance of hetero-atom doped iron-based sulfides electrocatalysts.

Catalyst	Doping element	Doping method	Working electrode substrate	Electrolyte	Overpotential @ current density (mV@mA/cm^2 @OER or HER)	Tafel slope (mV/dec)	Stability (h)	Ref.
Co-FeS_2	Co	Solvothermal	/	1.0 mol/L KOH	267@10@HER 324@10@HER	57	10	[112]
$Co_{13.6\%}$-Fe_7S_8	Co	Hydrothermal	/	1.0 mol/L KOH	311@10@OER, 284@10@HER	50@OER, 88@HER	10	[113]
$Fe_{0.39}Co_{0.61}S_2$/RGO	Co	Hot-injection	RGO	1.0 mol/L KOH	198@10@HER	94	/	[114]
$FeNi_{0.20}S_2$-RGO	Ni	Hydrothermal	RGO	0.5 mol/L H_2SO_4	183@10@HER	78	/	[115]
Ni-Fe-S	Ni	Hydrothermal	/	1.0 mol/L KOH	223@10@OER, 115@10@HER	41@OER, 108@HER	10	[116]
Mo-FeS	Mo	Hydrothermal	/	1.0 mol/L KOH	210@10@OER	50	30	[117]
N-FeS_2	N	NH_3 treatment	/	1.0 mol/L KOH	126@10@HER	124	20	[118]
6B-Fe_7S_8/FeS_2	B	$NaBH_4$ Boronation	CC	1.0 mol/L KOH	113@10@HER	57	30	[119]
P/Co-FeS_2	P, Co	CVD	CFP	0.5 mol/L H_2SO_4	90@100@HER	41.5	156	[120]

the surface is weakened, which facilitates the desorption of H_2 at the surface. Furthermore, the ΔG_{H^*} value on the pure FeS_2 surface is 0.046 eV, and the N-doping reduces the ΔG_{H^*} value to 0.029 eV, which is much closer to zero. Therefore, it can be seen that N doping enhances the intrinsic activity of FeS_2.

In contrast to N dopant, electron-deficient B dopant is also known to be an effective strategy to optimize the electronic structure of iron sulfide nanomaterials and promote their intrinsic electrocatalytic activity. Wu *et al.* [119] synthesized boron-doped Fe_7S_8/FeS_2 (B-Fe_7S_8/FeS_2) electrocatalysts on carbon cloth on the basis of DFT calculation and studied the effect of boron doping on the catalytic reaction mechanism firstly. Subsequently, it was demonstrated that the catalysts with optimal B-atom doping showed exceptional catalytic activity for HER (Figs. 4d and e) in alkaline media (113 mV@10 mA/cm^2), which was superior to most reported iron-based sulfide electrocatalysts. Mechanistic studies have shown (Figs. 4f-i) that doping an appropriate amount of boron atoms in the Fe_7S_8/FeS_2 system can modulate the position of the d-band center of the Fe atom and the p-band center of the S atom, which increase the electron density near the fermionic energy level and accelerate the charge transfer rate in the catalytic process, thus reducing the hydrolysis energy barrier and the hydrogen adsorption free energy (ΔG_{H^*} value of only −0.103 eV), thereby obtaining excellent HER electrocatalytic performance.

Optimizing the electronic structure and surface composition of iron-based sulfides by co-doping metal atoms and anions to promote the adsorption/desorption of intermediates is another effective strategy to improve the catalytic performance of iron-based sulfides. Kuo *et al.* [120] successfully synthesized cobalt/phosphorus co-doped FeS_2 nanocomposite (P/Co-FeS_2) through simple solvothermal, sulfurization and phosphating processes (Figs. 4j and k). P/Co-FeS_2 catalyst shows promising HER activity (90 mV@100 mA/cm^2) in 0.5 mol/L sulfuric acid solution, with a Tafel slope of 41.5 mV/dec, and maintains good durability during 156 h of HER with almost no significant change in surface structure (Figs. 4l and m). Co and P co-doping promote the adsorption process of adjacent hydrogen atoms and decrease the free energy of hydrogen adsorption, which can together enhance the catalytic activity of HER.

Table 2 summarizes the above heteroatom-doped iron-based sulfide electrocatalysts. As can be seen from the table, for the single-atom doped iron-based sulfide catalysts, the catalysts doped with Co atoms have the most excellent OER performance, while the B-doped catalyst has superior HER catalytic performance. Remarkably, the anionic and cationic co-doped P/Co-FeS_2 possesses the most excellent HER performance. Moreover, it was found that anionic doping usually improved the HER electrocatalytic performance of iron-based sulfides more than cationic doping, while cationic doping improved the OER performance better. This may be due to the fact that multi-metal doping increases the metal-centered catalytic active sites in the reaction, while anionic doping optimizes the electronic structure of the catalyst and promotes the improvement of the intrinsic catalytic performance. It is also evident from Table 2 that the hydrothermal method is commonly used in most atomic doping reactions due to its convenience of operation and controlled composition and structure. So far, most of the studies on improving the electrocatalytic performance of iron-based sulfides OER and HER using heteroatom doping methods have focused on cation doping. Therefore, in order to promote the improvement of the overall electrocatalytic performance of catalysts, anionic and cationic co-doping methods should be investigated more extensively and systematically.

5. Iron-based sulfide composites electrocatalysts for OER and HER

To further enhance the OER and HER activity of iron-based sulfide catalysts, iron-based sulfide is combined with other materials such as carbon, metal oxides, metal hydroxides, metal sulfides and other materials to form nanocomposites. This sub-section will present a detailed description of these different types of iron-based sulfides electrocatalysts and their electrocatalytic properties.

5.1. Iron-based sulfides/carbon composites

It is well known that the excellent carbon-based materials are widely used to facilitate charge transfer and provide effective active sites in catalysts, which are attributed to their high electrical conductivity, large surface area and robust mechanical properties. Consequently, the construction of iron sulfide with carbon nanohybrids is an effective strategy to improve their OER and HER performance. Carbon substrates mainly include N-doped carbon nanotubes (NCNT), porous graphene, MXene and carbon nanosheets (CN).

For instance, Xie *et al.* [121] designed and synthesized a novel type of ultra-miniature FeS_2 NPs distributed on MXene nanosheets (FeS_2@MXene) through a refined adsorption-growth pathway. The MXene material as a substrate effectively prevents the aggregation of FeS_2 NPs, thus exposing more active sites. Furthermore, the interface formed by FeS_2 and MXene has strong electronic interactions, which facilitates the contact between active sites and electrolyte solution, resulting in improving catalytic activity and stability. In Fig. 5a, distinct FeS_2 NPs can be observed on the MXene nanosheets. With the benefit of interfacial effect and unique three-dimensional structure, the prepared FeS_2@MXene catalysts exhibit excellent electrocatalytic performance for both OER (240 mV@10 mA/cm^2) and HER (87 mV@10 mA/cm^2) in alkaline solution. Additionally, it was found by *in situ* Raman spectroscopy (Fig. 5b) that

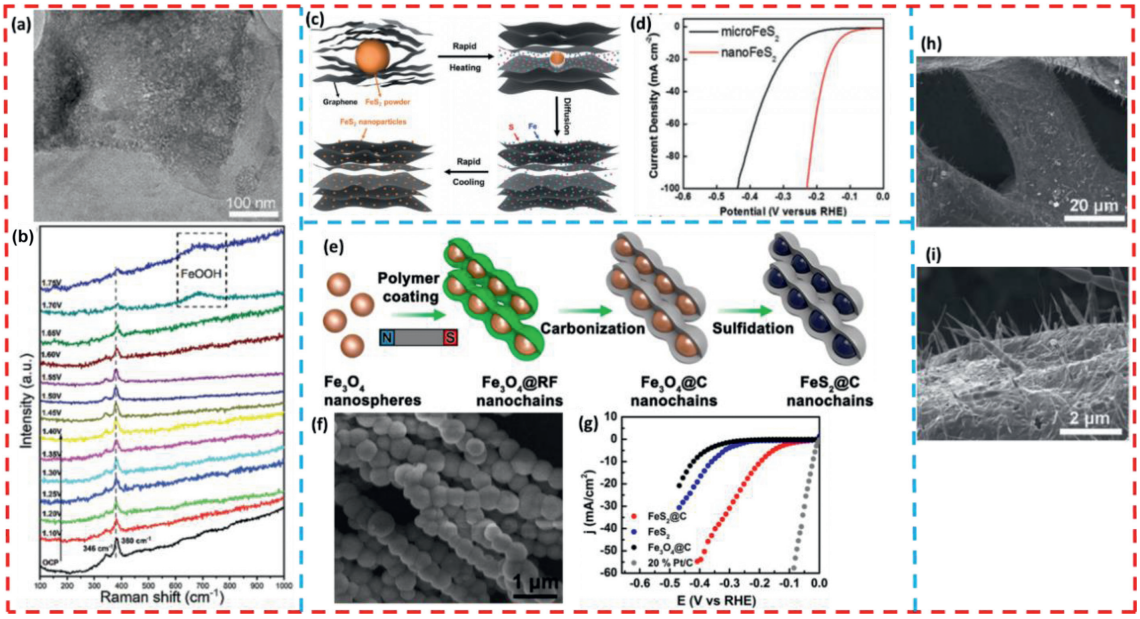

Fig. 5. (a) TEM of FeS_2@MXene. (b) *In situ* Raman spectra of the FeS_2@MXene catalyst at various potentials for OER processes. Copied with permission [121]. Copyright 2022, The Royal Society of Chemistry. (c) Schematic illustration of the ultrafast, *in situ* transformation of minerals to catalyst nanoparticles. (d) The HER polarization curves of nano-FeS_2-RGO in comparison to micro-FeS_2-RGO in 0.5 mol/L H_2SO_4. Copied with permission [122]. Copyright 2017, Wiley-VCH GmbH. (e) Schematic illustration of the synthesis process of FeS_2@C nanochains. (f) SEM images of FeS_2@CS-40 material. (g) LSV curves for all electrocatalysts. Copied with permission [123]. Copyright 2019, American Chemical Society. (h) Low-resolution SEM and (i) high-resolution SEM images of the FeS foams with surface grown carbon nanotube arrays. Copied with permission [124]. Copyright 2020, The Royal Society of Chemistry.

FeOOH as the active material enhanced the intrinsic activity of the catalyst in the OER process.

Chen *et al.* [122] constructed ultrafine FeS_2 NPs (FeS_2@RGO) which were uniformly distributed on reduced graphene oxide by utilizing a high-temperature rapid thermal shock technique (Figs. 5c and d). The 3-D structure consisting of embedded grown FeS_2 NPs and two-dimensional reduced graphene oxide nanosheets effectively ensures the electrical conductivity and high surface area of the composite, and accelerates ion diffusion and electron transfer. With these advantages, the FeS_2@RGO composite nanomaterials are used as efficient and stable HER electrocatalysts. The low overpotential is 139 mV in 0.5 mol/L sulfuric acid solution when the current density is 10 mA/cm^2.

In addition, a carbon layer as support is also an effective solution to enhance electroconductivity and improve the active sites of the material. Fan *et al.* [123] successfully synthesized FeS_2 nanochains (FeS_2@C) which were encapsulated by a uniform carbon layer with a magnetic-field-guided interface co-assembly method. This unique core-shell structure is formed (Figs. 5e-g), it is first assembled into chains by polymer coating under a magnetic field environment, then follows by continuous carbonization and hydrothermal vulcanization process. It prevents iron disulfide nanoparticles from aggregating during the HER process, which exposes more active sites. Also, this increases specific surface area of the catalyst, which is beneficial to improve the charge/mass transfer efficiency. Moreover, the interfacial effect between FeS_2 NPs and carbon layer also enhance electrocatalytic activity. Consequently, FeS_2@C nanocomposites with a thickness of 40 nm are considered as an effective and stable HER electrocatalysts. At a current density of 10 mA/cm^2, only 195 mV overpotential is required to catalyze the hydrogen evolution reaction with stable persistence over 150 h.

Guo *et al.* [124] synthesized FeS foam precursors by an *in-situ* sulfidation process using thiourea as the sulfur source. Then, N-doped carbon nanotube arrays (FeS/NCNTs foam), which are catalyzed by FeS nanocrystals, are obtained on the surface of FeS foam by a simple annealing process (Figs. 5h and i). The NCNT material as a coating not only greatly improves the electrical conductivity and corrosion resistance of the ferrous sulfide foam, but also provides a unique superaerophobic structure for FeS foam, which reduces the solid-gas contact area at the electrode-bubble interface, effectively avoiding the adsorption of large bubbles on the electrode and exposing more active sites. A cell voltage of only 1.942 V is required to achieve a current density of 100 mA/cm^2 when applying the FeS/NCNTs foam electrode to overall water splitting.

5.2. FeS/metal oxides composites

Chen *et al.* [104] first prepared Fe_2O_3@C by a two-step hydrothermal reaction, and then synthesized γ-Fe_2O_3@FeS_2@C with a unique core-double shell heterogeneous nanostructure using sulfur powder as the sulfur source (Fig. 6a). As shown in Figs. 6b and c, the catalyst exhibited an overpotential of 268 mV in 1.0 mol/L KOH when 10 mA/cm^2 was reached, which was smaller than that of pure α-Fe_2O_3, α-Fe_2O_3@C and γ-Fe_2O_3@FeS_2. And the Tafel slope of γ-Fe_2O_3@FeS_2 was also lower than that of other pure catalysts, which indicated the unique dual interface of the core-double shell nano-heterostructure accelerated the rapid electron transfer and the electrochemical reaction of oxygen-containing intermediates, thus improving the OER performance.

Wang *et al.* [125] constructed a series of Fe_3O_4/FeS_2 composites with heterogeneous structures using an *in situ* sulfuration strategy (Figs. 6d and e). Among them, Fe_3O_4/FeS_2-2.5 provides excellent catalytic activity for OER. In alkaline electrolytes, a low overpotential of only 306 mV is required for a current density of 100 mA/cm^2. Moreover, it can keep a current of about 10 mA/cm^2 for 36 h without significant performance degradation, which indicates Fe_3O_4/FeS_2-2.5 has good durability (Fig. 6h). It is worth noting that XPS indicates that the charge at Fe and S is transferred to O, achieving a charge redistribution. As shown in Figs. 6f and g, DFT calculations also confirm that the charge redistribution at the interfacial region reduces the activation potential barrier of oxygen-

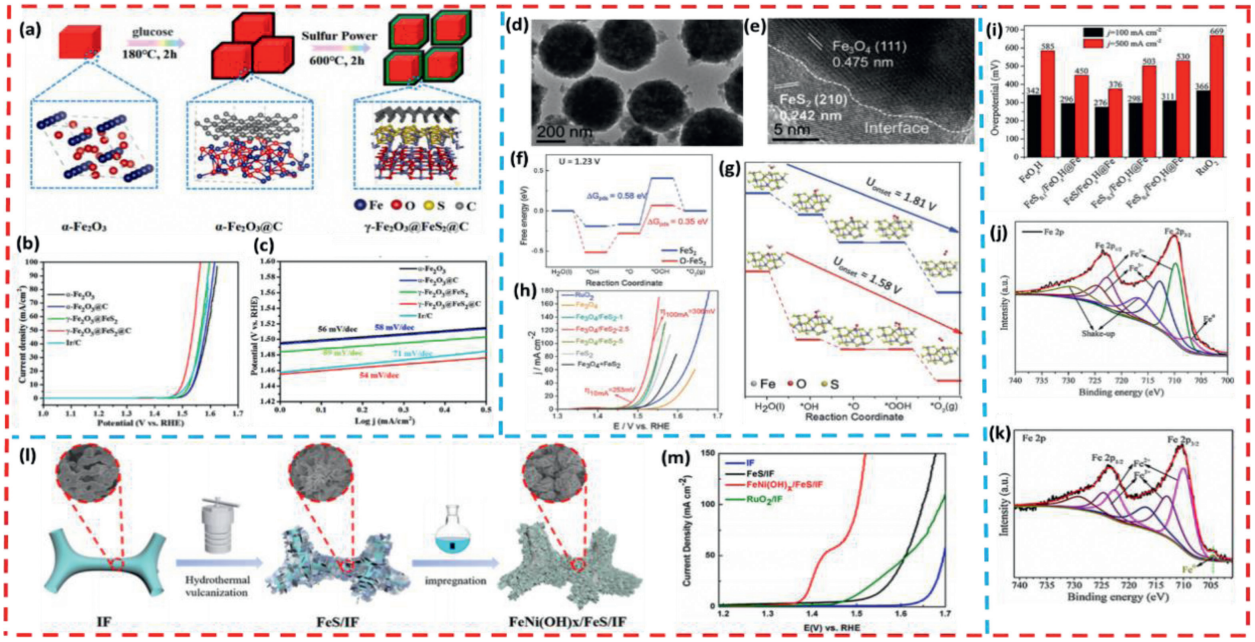

Fig. 6. (a) Schematic illustration of the formation of core-double shell heterostructure γ-Fe_2O_3@FeS_2@C nanocubics. (b) LSV curves. (c) Tafel plots of various catalysts for OER tests. Copied with permission [104]. Copyright 2021, Elsevier. (d, e) The HRTEM images for Fe_3O_4/FeS_2-2.5. The free energy diagram of (f) the OER process at 1.23 V and (g) at the onset potentials. (h) Polarization curves of different electrocatalysts (with IR correction). Copied with permission [125]. Copyright 2020, The Royal Society of Chemistry. (i) The overpotentials at 100 mA/cm^2 and 500 mA/cm^2 of the FeO_xH, $FeS_{0.1}$/FeO_xH@Fe, FeS/FeO_xH@Fe, $FeS_{0.3}$/FeO_xH@Fe, $FeS_{0.4}$/FeO_xH@Fe and Ni foam. (j, k) XPS of Fe 2p of FeS/FeO_xH@Fe before and after stability. Copied with permission [101]. Copyright 2022, Elsevier. (l) Schematic illustration of the synthesis process of $FeNi(OH)_x$/FeS/IF. (m) LSV curves of various samples. Copied with permission [126]. Copyright 2020, Elsevier.

containing intermediates, and thereby improving the catalytic performance of OER.

5.3. FeS/metal hydroxides composites

Tan *et al.* [101] successfully grow FeS/FeO_xH@Fe nanosheets with amorphous-crystalizes interface structure on Ni foams through a convenient one-step co-deposition method, which can be used as electrocatalytic electrodes for highly active and stable OER. FeS/FeO_xH@Fe exhibited excellent electrocatalytic activity in the OER process with current densities up to 500 mA/cm^2 and overpotentials as low as 376 mV (Fig. 6i). The outstanding catalytic performance of FeS/FeO_xH@Fe electrode might be attributed to the defective heterogeneous interface structure formed by FeS and FeO_xH which not only provided a larger active surface area and exposed more angular/edge active sites, but also promoted charge/mass transfer at the interface and facilitated the adsorption/desorption of bubbles. At the same time, according to the XPS results of Fe 2p before and after stability (Figs. 6j and k), the results showed that the binding energy was positively shifted, which was due to the significant changes in the electronic structure of the material surface during the stability test, and most of the FeS was converted to the active material FeOOH, which also further improved the OER catalytic activity.

Chen *et al.* [126] rationally constructed and prepared amorphous Fe-Ni bimetallic hydroxide films ($FeNi(OH)_x$/FeS/IF) grown vertically on three-dimensional and conductive FeS/IF nanosheets through an ultrafast surface modification process (Figs. 6l and m). Firstly, they prepared FeS/IF precursors using a conventional hydrothermal vulcanization method, and then put them into a mixed solution of nickel nitrate and sodium nitrate at 100 °C for a rapid reaction of 30 s (ultra-fast surface modification process) to obtain amorphous Fe-Ni bimetallic hydroxide nanosheet films grown vertically on three-dimensional and conductive FeS/IF. The *in-situ* grown OER catalyst without a binder successfully solves the problems of poor stability and inefficiency. More importantly, the unique inter-cross-linked nanosheet structures exposes a larger active surface area and abundant active sites, as well as the synergistic effect of $Fe(OH)_x$ and $Ni(OH)_x$, which together improve the electrocatalytic performance of OER. As a result, the $FeNi(OH)_x$/FeS/IF catalyst exhibits a low overpotential of 273 mV at a current density of 100 mA/cm^2.

5.4. FeS/metal sulfides composites

By using NiFe-LDH/TM as the precursor material, Luan *et al.* [127] prepared FeS-NiS hetero-structured nanosheet arrays (FeS-NiS/TM) based on Ti mesh substrates by hydrothermal sulfidation strategy. The catalysts exhibited superior OER electrocatalytic activity and stability than pure FeS/TM and NiS/TM in alkaline conditions. Fig. 7a clearly shows the overlapping lattice stripes of FeS and NiS, which may have a synergistic effect and thus improve the electrocatalytic performance. The C_{dl} of the FeS-NiS/TM electrode (3.40 mF/cm^2) was higher than that of FeS/TM (1.28 mF/cm^2). Since the double-layered capacitance is proportional to the electrochemical active surface area (ECSA), FeS-NiS/TM has a larger active surface, which indicates the presence of more exposed active sites between the FeS and NiS interfaces, as well as the synergistic effect of the interfaces enhancing their catalytic reaction kinetics.

Pan *et al.* [128] successfully constructed a three-dimensional porous Ni-Fe sulfide (Ni-Fe-S/NF) nanosheet array structure on NF by a simple hydrothermal strategy (Fig. 7b). The catalyst requires only low overpotentials of 253 mV and 262 mV to achieve OER and HER at a current density of 100 mA/cm^2, respectively. Moreover, the excellent overall water splitting performance requires only 1.55 V and 1.75 V at 10 mA/cm^2 and 100 mA/cm^2, respectively, and is stable for about 100 h. As can be seen from the HRTEM (Figs. 7c and d), there are many small pores on the nanosheets, which expose more active sites and provide channels for electron transfer and mass transport. The three-dimensional porous nanosheet structure exposing a large number of active sites, as well as the

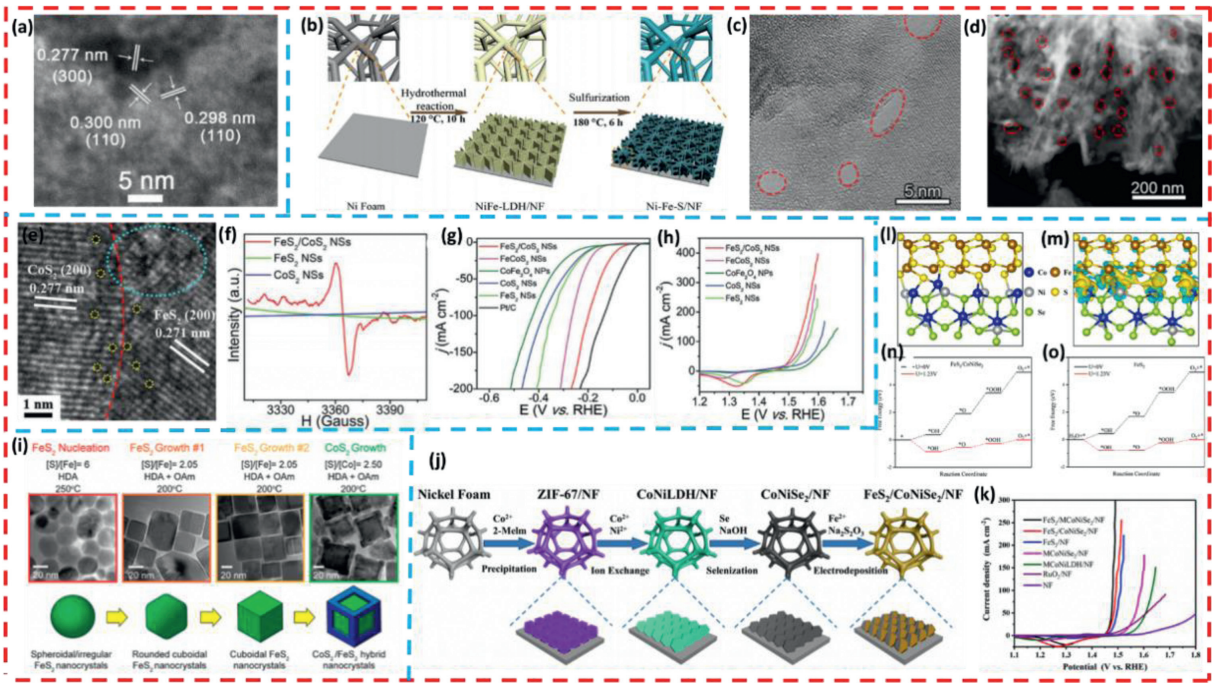

Fig. 7. (a) HRTEM image of FeS-NiS nanosheet. Copied with permission [127]. Copyright 2019, The Royal Society of Chemistry. (b) Schematic illustration for the synthesis of 3D porous Ni-Fe-S/NF. (c) HRTEM and (d) HAADF-STEM of Ni_3S_2-FeS/NF-2. Copied with permission [128]. Copyright 2022, Elsevier. (e) HRTEM image of FeS_2/CoS_2 NSs, the dotted circles and large oval represent defects and disordered structure, respectively. (f) EPR spectra of FeS_2/CoS_2 NSs, FeS_2 NSs, and CoS_2 NSs. LSV curves of different electrocatalysts for (g) HER and (h) OER. Copied with permission [129]. Copyright 2018, Wiley-VCH GmbH. (i) Schematic fabrication of the synthesis of CoS_2/FeS_2 hybrid nanocrystals. Copied with permission [130]. Copyright 2018, American Chemical Society. (j) Schematic of illustration of the $FeS_2/CoNiSe_2$ on NF. (k) LSV polarization curves of various electrocatalysts. (l) Model structure of $FeS_2/CoNiSe_2$. (m) The differential charge densities of $FeS_2/CoNiSe_2$ (the yellow and blue regions represent electron accumulation and depletion, respectively). (n, o) Free energy profiles for $FeS_2/CoNiSe_2$ and FeS_2 at zero potential ($U = 0$ V) and equilibrium potential for oxygen evolution ($U = 1.23$ V). Copied with permission [132]. Copyright 2018, The Royal Society of Chemistry.

strong electronic interactions and synergistic effects between Ni_3S_2 and FeS, resulting in excellent electrocatalytic properties and good durability.

By using $CoFe_2O_4$ nanoparticles prepared by a simple co-precipitation method as precursors, Li *et al.* [129] successfully synthesized FeS_2/CoS_2 nanosheets by chemical transformation strategy. It can be seen from the HRTEM image of FeS_2/CoS_2 nanosheets in Fig. 7e that the homogeneous nanosheets have a clear two-phase interface and many defects, which may be attributed to the generation of S vacancies. The electron paramagnetic resonance spectra in Fig. 7f precisely demonstrate this point, that the FeS_2/CoS_2 nanosheets have a strong EPR signal compared to other samples. As a result of the heterogeneous interfacial disordered structure and abundant sulfur vacancy defects of FeS_2/CoS_2 in the nanosheets, the catalysts obtain more fully exposed active sites and the best reaction kinetics for the overall water splitting. Due to these advantages, the FeS_2/CoS_2 NSs electrode exhibits high electrocatalytic activity for OER (302 mV@100 mA/cm^2) and HER (78.2 mV@10mA/cm^2) and superior stability (80 h@10mA/cm^2@HER) in 1.0 mol/L KOH solution (Figs. 7g and h). More importantly, the FeS_2/CoS_2 NSs electrodes composed of overall water splitting device requires only 1.47 V cell voltage to achieve a current density of 10 mA/cm^2 and maintains more than 21 h.

Jordan *et al.* [130] reported a FeS_2/CoS_2 core-framework nanostructure as an efficient and stable HER electrocatalyst (Fig. 7i). It is observed by the 3-D rendering technique that CoS_2 acts as the outer framework wrapping the FeS_2 nanoparticles, and this unique structure provides sufficient stability and porosity for the catalyst. At the same time, the catalyst also possesses a large active specific surface area, which enrich the active sites on the catalyst surface. Compared with pure FeS_2, FeS_2/CoS_2 core-framework nanocomposites exhibit superior HER activity in acidic electrolyte solution.

Wang *et al.* [131] prepared Co-FeS_2/CoS_2 heterostructure electrocatalysts on carbon cloth (CC) using a facile hydrothermal method. The prepared catalyst has a unique three-dimensional layered nanostructure and exhibits excellent electrocatalytic activity for OER and HER. The authors concluded that the improved electrocatalytic performance could be attributed to the following reasons: (1) Co doping decreased the reaction potential barrier of FeS_2 and enhanced its intrinsic catalytic activity; (2) The unique three-dimensional layered nanostructure resulted in a high specific surface area, as well as the raised heterogeneous structure of CoS_2 further exposed more active sites that could contact with electrolyte ions and promoted the adsorption and desorption of bubbles; (3) The synergistic effect between the two phases of CoS_2 and FeS_2 further enhanced the electrocatalytic activity; (4) It was further demonstrated by DFT calculations that sulfur was the real active site of the catalytic reaction, while the combination of the two phases resulted in a lower free energy of hydrogen adsorption, which theoretically demonstrated the good catalytic kinetics of the Co-FeS_2/CoS_2 nanocomposite.

Yang *et al.* [132] designed and prepared a heterostructure consisting of FeS_2 and MOF-derived $CoNiSe_2$ ($FeS_2/MCoNiSe_2$) as an excellent OER electrocatalyst (Figs. 7j and k). When it is applied to 1.0 mol/L KOH electrolyte for OER testing, only an overpotential of 230 mV is required to drive a current density of 10 mA/cm^2, and it can be stable for about 45 h. The outstanding electrocatalytic performance is mainly attributed to the electron coupling at the heterogeneous interface of $FeS_2/MCoNiSe_2$, which is indicated by the theoretical calculations (Figs. 7l-o). The electron transfer from $CoNiSe_2$ to the vicinity of FeS_2 according to the analysis in Figs. 6a and b, which indicates a reduction of the water adsorption energy. In addition, in Figs. 6c and d, the ΔG_{H^*} value of pure FeS_2 is calculated to be 0.52 eV, and the ΔG_{H^*} value after constructing het-

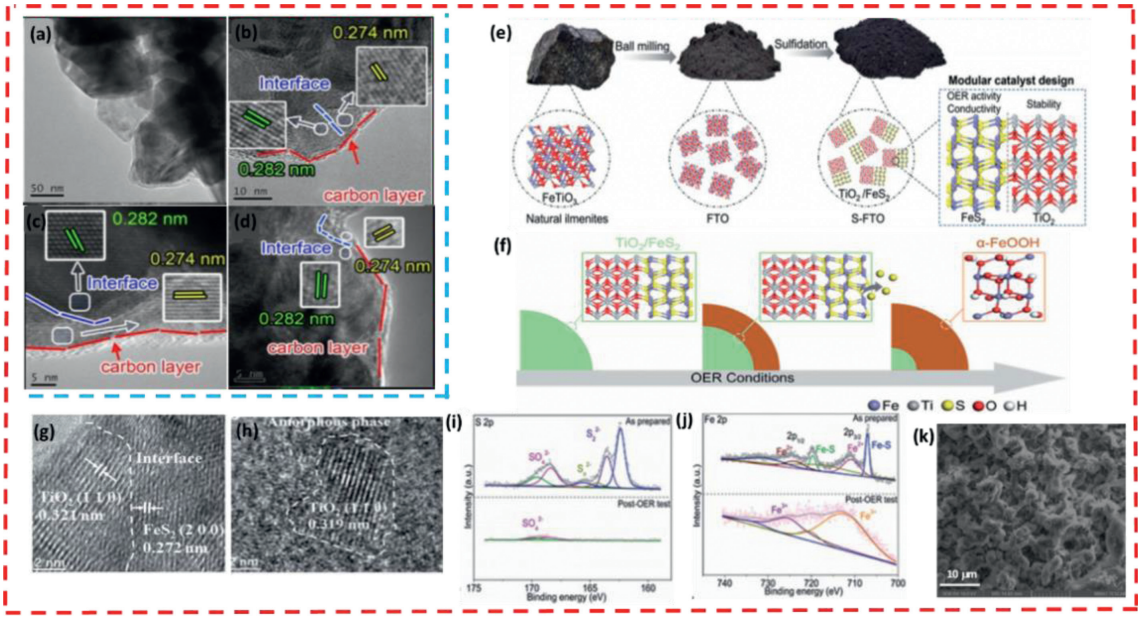

Fig. 8. (a-d) TEM and HAADF-STEM images of the carbon-layer-coated CoS_2-FeS_2 heterojunction nanosheets. Copied with permission [133]. Copyright 2020, The Royal Society of Chemistry. (e) Schematic illustration of the synthesis of FeS_2/TiO_2. (f) Illustration of the proposed surface evolution process of FeS_2/TiO_2 under OER conditions. (g, h) HRTEM images of S-FTO before and after OER test, respectively. (i) S 2p and (j) Fe 2P regions before and after the OER test. Copied with permission [134]. Copyright 2021, The Royal Society of Chemistry. (k) SEM images of PU@PANI@FeS_2 nanocomposites. Copied with permission [135]. Copyright 2020, Elsevier.

erojunction FeS_2/$MCoNiSe_2$ is reduced to 0.31 eV, which indicates that FeS_2/$MCoNiSe_2$ has faster electrochemical kinetics and better OER catalytic activity. Meanwhile, according to the analysis of the density of states (DOS) results, FeS_2/$MCoNiSe_2$ has a higher DOS near the Fermi energy level compared with FeS_2, which significantly improves the conductivity. As shown above, the construction of FeS_2 and $CoNiSe_2$ into a heterogeneous structure reduces the potential barrier of the OER reaction process and enhances the electron transfer rate at the heterogeneous interface.

Wang *et al.* [133] proposed a simple one-pot method to develop an amorphous carbon layer-coated CoS_2-FeS_2 heterojunction nanosheet bifunctional electrode (Figs. 8a-d). The prepared carbon-layer-coated CoS_2-FeS_2 composite nanomaterial has the following structural properties and advantages: (1) The amorphous carbon layer can change the chemical state of the CoS_2-FeS_2 nanosheet surface and accelerate the electron transfer rate of water, thus improving the electrical conductivity of the electrode; (2) The heterojunction interface formed between CoS_2 and FeS_2 exposes more active sites, meanwhile, the synergistic effect of CoS_2 and FeS_2 at the interface modulates their electronic structure and promotes the electron transfer between the electrolyte solution and the electrode; (3) The carbon-layer coated CoS_2-FeS_2 nanocomposite has excellent OER and HER catalytic performance and long-term stability in 1.0 mol/L KOH. This low-cost and highly efficient bifunctional catalyst offers promising applications. It requires only a low overpotential of 147 mV and 210 mV for OER and HER, respectively, to drive a current density of 10 mA/cm^2. It is worth noting that only 1.66 V of cell voltage is required at a current density of 10 mA/cm^2 in its composition of a two-electrode device and has been tested for 26 hours of durability.

5.5. FeS/other materials composites

Chen *et al.* [134] rationally designed and synthesized an efficient and stable hetero-structured FeS_2/TiO_2 (S-FTO) electrocatalyst using titanite (FTO) as raw material through a simple sulfuration treatment (Fig. 8e). S-FTO exhibits excellent OER activity and long-term durability in a 1.0 mol/L KOH electrolyte with a potential of 230 mV (10 mA/cm^2), which is much better than the pristine FTO. To further understand the conformational relationship between the electronic properties-catalytic activity of the catalyst surface during OER, the authors use S-FTO as a model material and analyzed its structural transformation after *i-t* testing. The significantly enhanced OER activity of the dynamically self-optimized 24h-S-FTO (FeS_2/TiO_2@FeOOH) compared with the original 0h-S-FTO can be attributed to the following reasons (Figs. 8f-j): (1) During the OER process, the S-FTO morphology changes remarkably, and the abundant nanoparticles expand the catalyst/electrolyte contact area; (2) After OER, the massive leaching of S elements not only induce the catalyst surface reconstruction and *in situ* generation of new active sites FeOOH, but also regulate the surface electronic structure and accelerate the charge/mass transfer; (3) The OER process promotes the *in-situ* generation of the core-shell structure FeS_2/TiO_2@FeOOH, with FeS_2/TiO_2 as the core ensuring high conductivity and long-term stability and FeOOH as the shell providing abundant active sites.

Since the inherent HER catalytic activity of iron disulfide is limited by low electrical conductivity and low surface area, Manjunatha *et al.* [135] reported a novel nanocomposite PU@PANI@FeS_2 by polymerizing and precipitating organic PANI (polyaniline) with FeS_2 nanoparticles on electrospun PU (polyurethane) nanofibers (Fig. 8k). The prepared catalyst shows excellent HER catalytic performance in 1.0 mol/L KOH electrolyte (265 mV@10 mA/cm^2, 372 mV@50 mA/cm^2), while PANI and PU improve their electrical conductivity and long-term durability. In addition, the one-dimensional PU nanofibers with FeS_2 nanoparticles make the surface with high porosity and high specific surface area, which is favorable for charge/electrolyte transfer, thus contributing to the enhancement of HER catalytic activity.

The iron-based sulfide composites are summarized in Table 3. It can be observed that the hetero-structured catalysts constructed from Ni_3S_2 and FeS have the best OER catalytic performance, while the hetero-structured catalysts fabricated by FeS_2 and CoS_2 have the best HER catalytic performance. It can also be noted that heterogeneous catalysts composed of iron-based oxides/hydroxides and iron-based sulfides exhibit good catalytic properties at high

Table 3
Performance of iron-based sulfide composites electrocatalysts.

Species	Electrocatalyst	Working Electrode Substrate	Electrolyte	Overpotential @ Current density (mV@mA/cm^2 @OER or HER)	Tafel slope (mV/dec @OER or HER)	Stability (h)	Ref.
Carbon	FeS_2@MXene	Mxene	1.0 mol/L KOH	87@10@HER, 240@10@OER, 1.57V@overall	58.6@OER, 97.7@HER	30	[121]
	FeS_2-RGO	RGO	0.5 mol/L H_2SO_4	139@10@HER	64@HER	10@24 mA/cm^2	[122]
	FeS_2@C	/	1.0 mol/L KOH	195@10@HER	128@HER	150	[123]
	FeS/NCNTs foam	NCNTs	1.0 mol/L KOH	1.942V@100@overall	/	50@100 mA/cm^2	[124]
Metal oxides	γ-Fe_2O_3@FeS_2@C	/	1.0 mol/L KOH	268@10@OER, 308@50@OER	54@OER	10@50 mA/cm^2	[104]
	Fe_3O_4/FeS_2	/	1.0 mol/L KOH	306@100@OER	48@OER	36@100 mA/cm^2	[125]
Metal hydroxides	FeS/FeO_xH@Fe	Ni foam	1.0 mol/L KOH	376@500@OER	71@OER	36@1000 mA/cm^2	[101]
	FeNi$(OH)_x$/FeS/IF	Iron foam	1.0 mol/L KOH	273@100@OER	53@OER	10	[126]
Metal sulfides	FeS–NiS/TM	Ti mesh	1.0 mol/L KOH	260@10@OER	80@OER	25	[127]
	Ni_3S_2-FeS/NF	Ni foam	1.0 mol/L KOH	253@100@OER, 262@100@HER	48@OER	100@100 mA/cm^2	[128]
	FeS_2/CoS_2	/	1.0 mol/L KOH	302@100@OER, 78.2@10@HER	42@OER, 44@HER	21	[129]
	FeS_2@CoS_2	/				/	[130]
	Co–FeS_2/CoS_2	Carbon cloth	0.5 mol/L H_2SO_4	278@10@OER, 103@10@HER	73@OER, 56@HER	/	[131]
	FeS_2/$CoNiSe_2$/NF	Ni foam	1.0 mol/L KOH	230@10@OER	54@OER	45	[132]
	CoS_2-FeS_2	/	1.0 mol/L KOH	147@10@OER, 210@10@HER	46@OER, 105@HER	26	[133]
Others	FeS_2/TiO_2	/	1.0 mol/L KOH	230@10@OER, 270@100@OER	47@OER	24	[134]
	PU@PANI@FeS_2	/	0.5 mol/L H_2SO_4	265@10@HER, 372@50@HER	15@OER	/	[135]

current densities and have been extensively studied. The overpotential at 10 mA/cm^2 current density is not reported in some literature due to the presence of oxidation peaks of pre-catalytic sulfides in OER tests, which makes the comparison of electrocatalytic performance more difficult.

In conclusion, simple and effective design principles and strategies need to be developed for better OER and HER performance of iron-based sulfides. In fact, two main strategies are used to improve their electrochemical properties: (1) exposing more accessible active sites; (2) changing their electronic structure to increase the intrinsic electrical conductivity. To achieve these goals, the following approaches are mainly used: heteroatom doping, composite design and generation of vacancy defects. In many works, heteroatom doping has been well established as an important and effective method to boost the intrinsic catalytic activity of iron-based sulfides, which is achieved by optimizing the surface electronic structure, increasing the free energy of adsorption of oxygenates and decreasing the free energy of hydrogen adsorption (ΔG_{H^*}). It is mainly divided into metal doping and anion doping, with transition metals Ni, Co and Mo as the main doping elements. Meanwhile, the doping methods are diverse, combining with hydrothermal method to add the salt of target doping atoms in the reaction precursor is a relatively simple method at present. Composite design, mainly divided into the construction of heterostructures or composites, is another attractive strategy for designing high-performance iron-based sulfide electrocatalysts currently. It is mainly used to construct heterogeneous interfaces or heterojunctions between iron-based sulfides and other materials resulting in changes of the surface electronic structure; meanwhile, integrating the unique physicochemical properties of two or more materials to jointly optimize the OER and HER performances. Normally, metal sulfides, oxides and hydroxides as well as carbon materials with excellent properties such as high electrical conductivity are selected to construct a high-performance system with iron-based sulfides. Sulfur vacancy defects are generally produced in iron-based sulfides, which can not only effectively modulate the adsorption/desorption free energy and improve the intrinsic activity of electrocatalysts, but also directly participate in the adsorption and electron transfer processes as active sites. Moreover, sulfur vacancies can also effectively modulate the electronic structure of active sites, influence the energy band structure and improve the conductivity.

6. The catalytic mechanism of iron-based sulfides electrocatalysts

For basic OER, the reaction mechanism:

$$M^* + OH^- \rightarrow M^*\text{-}OH + e^- \quad (1)$$

$$M^*\text{-}OH + OH^- \rightarrow M^*\text{-}O + H_2O(g) + e^- \quad (2)$$

$$M^*\text{-}O + OH^- \rightarrow M^*\text{-}OOH + e^- \quad (3)$$

$$M^*\text{-}OOH + OH^- \rightarrow M^* + O_2(g) + H_2O(l) + e^- \quad (4)$$

$$2M^*\text{-}O \rightarrow 2M^* + O_2(g) \quad (5)$$

There are usually two types of OER pathways. However, iron-based sulfides usually follow the first route as Eqs. 1-4. At first, the catalyst (M*) adsorbs OH^- in the electrolyte to form M*-OH, which subsequently reacts with OH^- to form M*-OO, which in turn reacts with OH^- to form M*-OOH intermediate, and finally M*-OOH reacts with OH^- to form O_2. For example, FeS_2/$MCoNiSe_2$/NF NSs reported by Yang *et al.* [132]. As shown in Figs. 7l-o, the Fe atoms on the catalyst surface absorb the hydroxide in the KOH electrolyte to form *OH, then *OH is deprotonated to form *O, *O combines with another OH^- to form *OOH, and then *OOH combined with OH^- is decomposed to OO* desorbed from the Fe atoms to form O_2. It is shown by theoretical calculations that FeS_2/$MCoNiSe_2$, which forms a heterogeneous interfacial structure, has a lower reaction energy barrier as well as a faster electron transfer rate compared to pure FeS_2. For example, when FeS_2/C NPs were used as OER electrocatalysts as reported by Li *et al.* [105], OH^- in 1.0 mol/L KOH was adsorbed on Fe sites to form FeS_2-OH; *O preferentially bound

to Fe sites to form Fe-O bonds on the FeS_2 surface. Finally, the active intermediates (*OH, *OOH and *O) combine with FeS_2 to produce O_2.

7. Conclusions and perspectives

This paper reviews the research progress and prospects of iron-based sulfide materials as OER and HER electrocatalysts. The synthesis methods of some iron-based sulfides and their composites, various nano-morphologies and their effects on catalytic performance are discussed. The above strategies have some application value and significance for the construction of novel and efficient iron-based sulfide electrocatalysts.

Based on the progress of iron-based sulfide catalysts in electrocatalytic OER and HER applications, we summarize the following points: (1) For pristine iron-based sulfide materials, modulation of mesoporous and hollow morphology can effectively improve electrocatalyst activity; (2) For heteroatom-doped electrocatalysts, atomic doping of metallic cobalt and molybdenum as well as nonmetallic boron can achieve greater catalytic performance improvement. However, most of the current atomic doping methods are hydrothermal methods, which are too single. Other doping methods and multi-element doping should be explored and tried, which may have unexpected results; (3) For the construction of catalysts with heterogeneous structures, the synergistic effect of each component in the electrocatalyst should be used reasonably. By taking advantage of the excellent electrical conductivity of iron-based sulfides and combining them with materials that have excellent catalytic properties and stability, highly active and long-lasting stable electrocatalysts can be constructed.

However, we should recognize that the practical application of iron-based sulfide electrocatalysts in OER and HER is still in its early stages and facing many challenges.

(1) More studies are needed to further reveal the contribution of iron-based sulfide electrocatalysts to the key steps of electrocatalysis and to illuminate the conformational relationships between composition-structure-performance, which would facilitate a wider range of catalysts in OER and HER applications. And, at present, the mechanism of electrocatalytic OER and HER reactions in water electrolysis by electrocatalysts has not been fully explained. Therefore, it is necessary to invest in multifaceted theoretical studies to reveal the real reaction mechanism at the atomic level so as to provide strong theoretical support for the development of excellent electrocatalysts.

(2) For heteroatom-doped iron-based sulfides, the main doping elements are still Ni, Co and N, *etc.* However, in order to further realize this strategy, more elements need to be explored to optimize the electronic structure of iron-based sulfide electrocatalysts. Consequently, more insight into the mechanisms involved in atomic doping is needed to facilitate the rational design of OER and HER electrocatalysts. In addition, there are few reports on iron-based sulfides with V as dopant, which will be a potential direction for their further development.

(3) Synergistic effect. It has been found empirically that iron-based sulfide electrocatalysts designed by just one strategy of increasing the number of active sites or increasing the intrinsic activity of the active sites are not sufficient to compete with noble metal electrocatalysts [136]. Hence, how to realize the organic combination of multiple strategies in theory and practice will become a new direction for us to investigate.

(4) Surface electrochemical reconstruction. At present, a large number of studies have suggested that iron-based sulfides only act as "pre-catalysts" and that reduction and amorphization occur during the electrochemical activation process. For this reason, it is important to discuss the surface reconstruction in OER and HER processes. It is necessary to gain more in-depth understanding of what "by-products" are generated on the Fe-based sulfide catalyst surface during electrochemical activation and how they affect the final Fe-based sulfide OER and HER electrocatalytic activity, since the steady-state electrocatalyst performance is assessed by the reconstructed electrode surface rather than by volume. At present, few theoretical studies have focused on how surface reconstruction affects the OER and HER activities of iron-based sulfide electrocatalysts, and the actual active sites of iron-based sulfides in the OER and HER processes as well as the catalytic mechanisms. Therefore, great efforts and research are needed in this field.

(5) Currently, many efforts are mainly concentrated on the construction of iron-based sulfides and their composite nanomaterials with good morphology and thus excellent electrocatalytic properties. However, their catalytic mechanisms have been little attention. Consequently, more attention should be paid to the dynamic processes on the catalyst surface during electrocatalytic reactions. Some of advanced modern *in-situ* characterization techniques are useful to uncover their catalytic mechanisms, such as *in-situ* simultaneous X-ray techniques, transmission electron microscopy techniques (3D reconstruction, five-dimensional reconstruction, spherical differential correction electron microscopy, and *in-situ* transmission electron microscopy), *in-situ* scanning probe techniques, *in-situ* XRD techniques, and *in-situ* Roman techniques. They may also reveal the transformation relationships between the species in the catalytic process, as well as more critical information that is relevant to intermediates and real active substances, and provide guidance for the design of catalysts.

(6) Density functional theory calculation is also an effective tool to deeply understand the conformational relationship between composition-structure-properties of nanomaterials. It can provide a more intuitive and accurate perspective of the whole electrocatalytic reaction process through simulating the theoretical crystal structure and calculating the adsorption energy and electronic density of states of the catalyst. Combining characterization techniques with theoretical calculations can help us to propose specific and effective modification strategies, which are important for improving the catalytic performance of iron-based sulfide materials and other non-precious metal-based materials.

In summary, although great progress has been made in iron-based sulfide nanomaterials for OER and HER, more research and exploration are needed to improve the catalytic performance and durability of iron-based sulfides at high current densities for eventual application in large-scale hydrogen production devices. Meanwhile, the currently reported iron-based sulfide electrocatalysts are mainly applied in alkaline electrolytes, while only a few of them have been employed in acidic and/or neutral media, which is mainly attributed to the susceptibility of iron-based sulfide electrocatalysts to corrosion and instability during long-term water electrolysis, thus severely limiting their practical applications in industry. Accordingly, there is an equal need to design and construct universal-pH bifunctional iron-based sulfide electrocatalysts with outstanding electrocatalytic activity and long-term durability in near-neutral media, as these would be of great significance for the large-scale development of seawater electrolysis industry. We believe that a rational design and modulation of the component-structure-property relationship, as well as an in-depth understand-

ing of the catalytic mechanism of iron-based sulfide materials will facilitate their further development as OER and HER electrocatalysts.

We expect that this review will stimulate more innovative ideas for the development of iron-based sulfides and other transition metal sulfide materials as OER and HER electrocatalysts.

Declaration of competing interest

We declare that we have no known competing financial interests or personal relationships that could have appeared to influence the work reported in this paper. There is no professional or other personal interest of any nature or kind in any product, service and/or company that could be construed as influencing the position presented in, or the review of, the manuscript entitled.

Acknowledgments

This work is supported by the National Natural Science Foundation of China (No. 22275052), and the Natural Science Foundation of Hubei Province (No. 2019CFB569). The authors would like to thank Shiyanjia Lab (www.shiyanjia.com) and SCI-Go (www.sci-go.com).

References

[1] D. Zhou, P. Li, W. Xu, et al., ChemNanoMat 6 (2020) 336–355.
[2] X. Peng, Y. Yan, X. Jin, et al., Nano Energy 78 (2020) 105234.
[3] L. Ouyang, X. He, Y. Sun, et al., Inorg. Chem. Front. 9 (2022) 6602–6607.
[4] B.B. Gicha, L.T. Tufa, S. Kang, et al., Nanomaterials 11 (2021) 1388.
[5] K. Hansen, C. Breyer, H. Lund, Energy 175 (2019) 471–480.
[6] J. Yu, T.A. Le, N.Q. Tran, H. Lee, Chemistry 26 (2020) 6423–6436.
[7] F. Gao, J. He, H. Wang, et al., Nano Res. Energy 1 (2022) e9120029.
[8] D. Li, F. Ding, Mater. Today Adv. 8 (2020) 100079.
[9] C. Ye, L. Zhang, L. Yue, et al., Inorg. Chem. Front. 8 (2021) 3162–3166.
[10] Y. Li, H. Dong, L. Li, et al., Water Res. 192 (2021) 116850.
[11] D. Gielen, F. Boshell, D. Saygin, et al., Energy Strategy Rev. 24 (2019) 38–50.
[12] Z. Liu, Y. Du, R. Yu, et al., Angew. Chem. Int. Ed. 62 (2023) e202212653.
[13] Z. Chen, X. Duan, W. Wei, S. Wang, B.J. Ni, Nano Energy 78 (2020) 105270.
[14] M.Z. Jacobson, M.A. Delucchi, Z.A. Bauer, et al., Joule 1 (2017) 108–121.
[15] A. Hussain, S.M. Arif, M. Aslam, Renew. Sust. Energ. Rev. 71 (2017) 12–28.
[16] F. Dong, M. Wu, Z. Chen, et al., Nanomicro Lett. 14 (2021) 36.
[17] C. Hu, L. Zhang, J. Gong, Energy Environ. Sci. 12 (2019) 2620–2645.
[18] L. Xiong, K. Wang, D. Li, et al., FlatChem 21 (2020) 100161.
[19] S. Tu, Y. Guo, Y. Zhang, et al., Adv. Funct. Mater. 30 (2020) 2005158.
[20] A. Sobhani, M. Salavati-Niasari, Adv. Colloid Interface Sci. 287 (2021) 102321.
[21] F. Guo, M. Zhang, S. Yi, et al., Nano Res. Energy 1 (2022) e9120027.
[22] Z. Wu, J. Bai, F. Lai, et al., Sci. China Mater. 66 (2023) 2680–2688.
[23] X. Fang, X. Wang, L. Ouyang, et al., Molecules 27 (21) (2022) 7617.
[24] Y. Qiu, Z. Liu, Q. Yang, et al., Chem. Eur. J. 28 (2022) e202200683.
[25] K. Chen, G. Zhang, X. Li, X. Zhao, K. Chu, Nano Res. 16 (2023) 5857–5863.
[26] K.T. Møller, T.R. Jensen, E. Akiba, H.W. Li, Mater. Int. 27 (2017) 34–40.
[27] Z. Zhuang, Y. Li, R. Yu, et al., Nat. Catal. 5 (2022) 300–310.
[28] M. Yue, H. Lambert, E. Pahon, et al., Renew. Sust. Energ. Rev. 146 (2021) 111180.
[29] N.P. Brandon, Z. Kurban, Phys. Eng. Sci. 375 (2017) 20160400.
[30] V. Charles, A.O. Anumah, K.A. Adegoke, et al., Sustain. Mater. Technol. 28 (2021) e00252.
[31] F. Dawood, M. Anda, G. Shafiullah, Int. J. Hydrog. Energy 45 (2020) 3847–3869.
[32] J. Lin, Z. Peng, W. Yang, et al., Electrochim. Acta 392 (2021) 139071.
[33] J. Li, Z. Niu, C. Guo, M. Li, W. Bao, J. Energy Chem. 54 (2021) 434–451.
[34] J. Yan, Nat. Clim. Change 8 (2018) 560–561.
[35] W. Zhang, L. Cui, J. Liu, J. Alloys Compd. 821 (2020) 153542.
[36] H. Yi, S. Liu, C. Lai, et al., Adv. Energy Mater. 11 (2021) 2002863.
[37] Z. Zhuang, L. Xia, J. Huang, et al., Angew. Chem. Int. Ed. 62 (2023) e202212335.
[38] S.S. Siwal, W. Yang, Q. Zhang, J. Energy Chem. 51 (2020) 113–133.
[39] A. Kovač, M. Paranos, D. Marciuš, Int. J. Hydrog. Energy 46 (2021) 10016–10035.
[40] J. Wang, X. Yue, Y. Yang, et al., J. Alloys Compd. 819 (2020) 153346.
[41] C. Meng, Y. Cao, Y. Luo, et al., Inorg. Chem. Front. 8 (2021) 3007–3011.
[42] Y. Cao, T. Wang, X. Li, et al., Inorg. Chem. Front. 8 (2021) 3049–3054.
[43] G. Meng, H. Cao, T. Wei, et al., Chem. Commun. 58 (2022) 11839–11842.
[44] H. Sun, Z. Yan, F. Liu, et al., Adv. Mater. 32 (2020) 1806326.
[45] L. Sun, Y. Dang, A. Wu, et al., Nano Res. 16 (2023) 5733–5742.
[46] R. Li, Z. Bai, W. Hou, et al., Chin. Chem. Lett. 32 (2021) 4063–4069.
[47] H. Xu, H. Shang, C. Wang, Y. Du, Coord. Chem. Rev. 418 (2020) 213374.
[48] X. Wang, L. Zhang, CP. Liu, et al., J. Electrochem. 28 (2022) 2108501.
[49] H. Zhu, S. Sun, J. Hao, et al., Energy Environ. Sci. 16 (2023) 619–628.
[50] XZ. Song, WY. Zhu, XF. Wang, Z. Tan, ChemElectroChem 8 (2021) 996–1020.
[51] L. Zhang, J. Liang, L. Yue, et al., Nano Res. Energy 1 (2022) e9120028.
[52] ZH. Wang, XF. Wang, Z. Tan, XZ. Song, Mater. Today Energy 19 (2021) 100618.
[53] C. Wang, C. Li, J. Liu, C. Guo, Mater. Rep.: Energy 1 (2021) 100006.
[54] Y. Liu, D. Zhou, T. Deng, et al., ChemSusChem 14 (2021) 5359–5383.
[55] W. Li, Y. Deng, L. Luo, et al., J. Colloid Interface Sci. 639 (2023) 416–423.
[56] E. Chen, W. Xu, J. Chen, J. Warner, Mate. Today Adv. 7 (2020) 100076.
[57] W. Zhang, X. Qin, T. Wei, et al., J. Colloid Interface Sci. 638 (2023) 650–657.
[58] Z. Chen, W. Wei, B.J. Ni, Curr. Opin. Green Sustain. Chem. 27 (2021) 100398.
[59] F. Zhang, Y. Liu, L. Wu, et al., Mater. Today Phys. 27 (2022) 100841.
[60] Z. Zhuang, Y. Li, Y. Li, et al., Energy Environ. Sci. 14 (2021) 1016–1028.
[61] H. Zhang, X. Yang, H. Zhang, et al., Chem. Eur. J. 27 (2021) 5074–5090.
[62] D. Wang, Y. Song, H. Zhang, X. Yan, J. Guo, J. Electroanal. Chem. 861 (2020) 113953.
[63] Y. Yan, P. Wang, J. Lin, J. Cao, J. Qi, J. Energy Chem. 58 (2021) 446–462.
[64] D. Jiang, S. Xu, M. Gao, et al., Inorg. Chem. 60 (2021) 8189–8199.
[65] A. Badreldin, A.E. Abusrafa, A. Abdel-Wahab, ChemSusChem 14 (2021) 10–32.
[66] J. Wang, Y. Xie, Y. Yao, et al., J. Mater. Chem. A 5 (2017) 14758–14762.
[67] S. Kumaravel, K. Karthick, S.S. Sankar, et al., Sustain. Energy Fuels 5 (2021) 6215–6268.
[68] Y. Sun, T. Zhang, C. Li, K. Xu, Y. Li, J. Mater. Chem. A 8 (2020) 13415–13436.
[69] Z. Zheng, L. Lin, S. Mo, Small 14 (2018) 1800759.
[70] L. Zhang, L. Li, J. Liang, et al., Inorg. Chem. Front. 10 (2023) 2766–2775.
[71] Y. Li, Z. Dong, L. Jiao, Adv. Energy Mater. 10 (2020) 1902104.
[72] N. Attarzadeh, R. Nuggehalli, C.V. Ramana, JOM 74 (2022) 381–395.
[73] D. Li, L. Liao, H. Zhou, et al., Mater. Today Phys. 16 (2021) 100314.
[74] Y. Wang, B. Kong, D. Zhao, H. Wang, C. Selomulya, Nano Today 15 (2017) 26–55.
[75] Y. Zhao, J. You, L. Wang, W. Bao, R. Yao, Int. J. Hydrog. Energy 46 (2021) 39146–39182.
[76] M. Wang, L. Zhang, Y. He, H. Zhu, J. Mater. Chem. A 9 (2021) 5320–5363.
[77] J. Chen, L. Zhang, J. Li, et al., J. Mater. Chem. A 11 (2023) 1116–1122.
[78] J. Theerthagiri, S.J. Lee, A.P. Murthy, J. Madhavan, M.Y. Choi, Curr. Opin. Solid State Mater. Sci. 24 (2020) 100805.
[79] X. Peng, C. Pi, X. Zhang, et al., Sustain. Energy Fuels 3 (2019) 366–381.
[80] P. Chen, J. Ye, H. Wang, L. Ouyang, M. Zhu, J. Alloys Compd. 883 (2021) 160833.
[81] J. Joo, T. Kim, J. Lee, S.I. Choi, K. Lee, Adv. Mater. 31 (2019) e1806682.
[82] Y. Li, Z. Yin, M. Cui, et al., J. Mater. Chem. A 9 (2021) 2070–2092.
[83] Y. Guo, T. Park, J.W. Yi, et al., Adv. Mater. 31 (2019) 1807134.
[84] F. Li, L. Wang, G. Qu, et al., Chin. Chem. Lett. 33 (2022) 3909–3915.
[85] M. Gu, S.C. Wang, C. Chen, D. Xiong, FY. Yi, Inorg. Chem. 59 (2020) 6078–6086.
[86] H. Bandal, K.K. Reddy, A. Chaugule, H. Kim, J. Power Sources 395 (2018) 106–127.
[87] X. Zou, Y. Wu, Y. Liu, et al., Chem 4 (2018) 1139–1152.
[88] M. Yu, E. Budiyanto, H. Tüysüz, Angew. Chem. Int. Ed. 61 (2022) e202103824.
[89] K. Li, D. Feng, Y.J.C. Tong, ChemSusChem 15 (2022) e202200590.
[90] J. Yin, J. Jin, H. Lin, et al., Adv. Sci. 7 (2020) 1903070.
[91] S. Wang, L. Wang, L. Xie, et al., Nano Res. 15 (2022) 4996–5003.
[92] S. Rana, J.P. Biswas, S. Paul, A. Paik, D. Maiti, Chem. Soc. Rev. 50 (2021) 243–472.
[93] M. Yang, YN. Zhou, YN. Cao, et al., Appl. Mater. Today 20 (2020) 100692.
[94] R. Elakkiya, G. Maduraiveeran, Nanoscale 13 (2021) 14837–14846.
[95] M.M. Najafpour, S.M. Hosseini, Int. J. Hydrog. Energy 41 (2016) 22635–22642.
[96] D. Heift, Inorganics 7 (2019) 75–94.
[97] Z. Song, J. Yi, J. Qi, et al., Nano Res. 15 (2022) 4687–4692.
[98] C. Meng, Y. Gao, Y. Zhou, et al., Nano Res. 16 (2023) 6228–6236.
[99] M. Abu Sayeed, G.J. Millar, A.P. O'Mullane, ChemElectroChem 6 (2019) 3667–3673.
[100] N. Mushtaq, Z. Wang, H. Tabassum, et al., Dalton Trans. 51 (2022) 6285–6292.
[101] Y. Tan, X. Xu, Q. Li, et al., J. Colloid Interface Sci. 594 (2021) 575–583.
[102] J. Zhang, Y. Wu, H. Hao, et al., Electrochim. Acta 402 (2022) 139554.
[103] K. Pan, Y. Zhai, J. Zhang, K. Yu, Materials 12 (2019) 3364.
[104] K. Chen, R. Rajendiran, D.H. Lee, J. Diao, O.L. Li, J. Alloys Compd. 885 (2021) 160986.
[105] Z. Li, M. Xiao, Y. Zhou, et al., Dalton Trans. 47 (2018) 14917–14923.
[106] Y. Liu, N. Ran, R. Ge, et al., Chem. Eng. J. 425 (2021) 131642.
[107] X. Zhang, Y. Zhao, Y. Zhao, et al., Adv. Energy Mater. 9 (2019) 1900881.
[108] H. Chen, X. Liang, Y. Liu, et al., Adv. Mater. 32 (2020) 2002435.
[109] P. Zheng, Q. Liu, X. Peng, L. Li, J. Yang, Nano 15 (2020) 2050135.
[110] R. Miao, B. Dutta, S. Sahoo, J. Am. Chem. Soc. 139 (2017) 13604–13607.
[111] G. Wang, C. Jin, G. Zhang, et al., Dalton Trans. 50 (2021) 6333–6342.
[112] L. Gao, C. Guo, X. Liu, et al., New J. Chem. 44 (2020) 1711–1718.
[113] Y. Wu, Z. Meng, X. Fang, et al., Ceram. Int. 47 (2021) 26484–26491.
[114] M. Wang, W. Tang, S. Liu, et al., J. Alloys Compd. 862 (2021) 158610.
[115] J. Jiang, L. Zhu, H. Chen, et al., J. Alloys Compd. 775 (2019) 1293–1300.
[116] Z. Yin, S. Zhang, J. Li, et al., New J. Chem. 45 (2021) 12996–13003.
[117] Z. Shao, H. Meng, J. Sun, et al., ACS Appl. Mater. Interfaces 12 (2020) 51846–51853.
[118] J. Ye, Y. Zang, Q. Wang, et al., J. Energy Chem. 56 (2021) 283–289.
[119] J. Wu, Q. Zhang, K. Shen, et al., Adv. Funct. Mater. 32 (2022) 2107802.
[120] TR. Kuo, WT. Chen, HJ. Liao, et al., Small 13 (2017) 1603356.
[121] Y. Xie, H. Yu, L. Deng, et al., Inorg. Chem. Front. 9 (2022) 662–669.
[122] Y. Chen, S. Xu, Y. Li, et al., Adv. Energy Mater. 7 (2017) 1700482.

[123] M. Fan, L. Zhang, K. Li, et al., ACS Appl. Nano Mater. 2 (2019) 3889–3896.
[124] M. Guo, A. Qayum, S. Dong, et al., J. Mater. Chem. A 8 (2020) 9239–9247.
[125] M.J. Wang, X. Zheng, L. Song, et al., J. Mater. Chem. A 8 (2020) 14145–14151.
[126] QW. Chen, XY. Zhang, YW. Dong, et al., J. Alloys Compd. 835 (2020) 155298.
[127] X. Luan, H. Du, Y. Kong, F. Qu, L. Lu, Chem. Commun. 55 (2019) 7335–7338.
[128] Z. Pan, M. Yaseen, P.Kang Shen, Y. Zhan, J. Colloid Interface Sci. 616 (2022) 422–432.
[129] Y. Li, J. Yin, L. An, et al., Small 14 (2018) e1801070.
[130] J.M. Rhodes, J.R. McBride, J.E. Macdonald, Chem. Mater. 30 (2018) 8121–8125.
[131] K. Wang, W. Guo, S. Yan, H. Song, Y. Shi, RSC Adv. 8 (2018) 28684–28691.
[132] J. Yang, H. Xuan, J. Yang, et al., Appl. Surf. Sci. 578 (2022) 152016.
[133] W. Wang, Y. Xu, J. Yao, et al., Dalton Trans. 49 (2020) 13352–13358.
[134] Z. Chen, R. Zheng, S. Deng, et al., J. Mater. Chem. A 9 (2021) 25032–25041.
[135] C. Manjunatha, R.S. Patil, M. Sudeep, et al., Surf. Interfaces 18 (2020) 100445.
[136] H. Han, Y. Qiu, H. Zhang, et al., Sustain. Energy Fuels 6 (2022) 3008–3013.